Anthropogenic CO2 in the Southern Ocean: distribution and inventory at the Indo-Atlantic boundary (WOCE line I6)

Claire Lo Monaco, Nicolas Metzl, Alain Poisson, Christian Brunet, Bernard
Schauer

Anthropogenic CO$_2$ in the Southern Ocean: Distribution and inventory at the Indian-Atlantic boundary (World Ocean Circulation Experiment line I6)

Claire Lo Monaco, Nicolas Metzl, Alain Poisson, Christian Brunet, and Bernard Schauer

Laboratoire de Biogéochimie et Chimie Marines (LBCM/IPSL), Université Pierre et Marie Curie, Paris, France

[1]   The Southern Ocean, where various water masses are formed (mode, intermediate, deep, and bottom waters), has a high potential to absorb anthropogenic CO$_2$ (C^{ant}). However, most data-based and model estimates indicate low C^{ant} inventories south of 50°S. In order to investigate this paradox, the distribution of C^{ant} is estimated between South Africa and Antarctica (World Ocean Circulation Experiment (WOCE) line I6) based on a back-calculation technique previously used in the North Atlantic (Körtzinger et al., 1998) and adapted here for application in the Southern Ocean. At midlatitudes (30°–50°S), formation and spreading of mode and intermediate waters results in a deep penetration of C^{ant} (down to 2000 m). South of 50°S, significant concentrations of C^{ant} were estimated in Circumpolar Deep Water (>10 μmol/kg) and Antarctic Bottom Water (AABW) (20–25 μmol/kg). Higher concentrations are detected along the continental slope in AABW presumably formed in Prydz Bay compared to AABW of Weddell Sea origin. The distribution of C^{ant} obtained north of 50°S compares well with previous data-based and model estimates, but large disagreements are found in the south. However, although transient tracers are not used in the back-calculation technique employed here, the distribution of C^{ant} is remarkably well correlated with CFCs. We reevaluated the column inventories of C^{ant} for the Southern Ocean and found higher values at high latitudes (70–90 mol/m^2) compared to the subtropical/subantarctic region (40–80 mol/m^2). These results support the idea that deep and bottom water formation in the Southern Ocean is a key process in the natural sequestration of anthropogenic CO$_2$.

1. Introduction

[2]   Since the modernization of human activity, anthropogenic release of CO$_2$ in the atmosphere has increased in an exponential way to reach the rate of 6–7 Gt C/yr in the 1990s. It was estimated that 3 Gt C/yr remained in the atmosphere while 3–4 Gt C/yr were absorbed by the ocean and the continental biosphere [*Intergovernmental Panel on Climate Change*, 2001]. Estimating actual CO$_2$ budgets and fluxes between the different reservoirs (both the natural and anthropogenic component) is of primary importance in order to predict their evolution and quantify the consequences of the rising CO$_2$ on future climate. Current global ocean models predict that the total uptake of anthropogenic CO$_2$ (C^{ant}) by the ocean ranged between 1.5 and 2.1 Gt C/yr during the 1990s [*Orr et al.*, 2001]. One third to one half of the total ocean uptake was found to occur south of 30°S. However, large disagreements exist in this region where different models present dramatic differences in the distri-

bution of C^{ant}. Uncertainties attached to global models are difficult to estimate because data-based methods also present debatable results south of 50°S. Resolving the distribution of C^{ant} in the Southern Ocean is therefore highly relevant to reduce the large uncertainty in future atmospheric CO$_2$ and hence global warming [*Friedlingstein et al.*, 2003].

[3]   The sinking of various water masses in the Southern Ocean provides a pathway for C^{ant} to penetrate into the ocean interior. In midlatitudes (30°–50°S), deep winter mixing results in the formation of homogeneous water masses (mode and intermediate waters). Isolated from the atmosphere in summer time, these newly formed waters sink to intermediate depths (500–1500 m) and are taken in the circumpolar circulation or transported northward in tropical regions [e.g., *McCartney*, 1977; *Piola and Georgi*, 1982]. Data-based methods together with global ocean models generally agree to simulate a deep penetration of C^{ant} around 40°S associated with the spreading of mode and intermediate waters [e.g., *Gruber*, 1998; *Sabine et al.*, 1999; *Orr et al.*, 2001; *Ríos et al.*, 2003]. South of 50°S, most data-based methods estimate very little storage of anthro-

pogenic CO$_2$ [*Poisson and Chen*, 1987; *Gruber*, 1998; *Sabine et al.*, 1999; *Hoppema et al.*, 2001]. However, these findings are in contradiction with significant concentrations of CFCs observed along the continental slope and in Antarctic deep and bottom waters [e.g., *Mantisi et al.*, 1991; *Archambeau et al.*, 1998; *Meredith et al.*, 2001; *Orsi et al.*, 2002]. CFCs are injected into the deep Southern Ocean through spreading and mixing of dense waters formed at several places around Antarctica [e.g., *Gordon*, 1971; *Gill*, 1973; *Wong et al.*, 1998; *Rintoul and Bullister*, 1999; *Schodlok et al.*, 2001]. It is expected that C^{ant} also penetrates deeply into the Southern Ocean following the same pathway as CFCs. This hypothesis is supported by recent results from *McNeil et al.* [2001] and *Sabine et al.* [2002] showing a significant accumulation of C^{ant} along the Antarctic slope near the Adélie Land coast.

[4] This paper presents new estimates of anthropogenic CO$_2$ along 30°E in the Southern Ocean obtained using a back-calculation technique previously applied to the North Atlantic Ocean [*Körtzinger et al.*, 1998]. In the initial method, however, oxygen is assumed to be at full saturation in surface waters, which is definitely not the case in ice-covered regions of the Southern Ocean. The method was therefore modified in order to meet this specific requirement. Both the initial and modified version were applied on data collected during the Circulation et Ventilation dans l'Antarctique (CIVA)-2 cruise (WOCE line I6). Estimates of C^{ant} are compared with CFC-11 measured during the cruise and revised inventories of C^{ant} are proposed for this region. These results are then discussed with regard to C^{ant} concentrations and inventories obtained along the same line using a different data-based method.

2. Data Collection

[5] This study is based on observations collected in 1996 onboard the R/V *Marion-Dufresne* during the French cruise CIVA-2 conducted along 30°E between South Africa and Antarctica (WOCE line I6). Among the 96 conductivity-temperature-depth (CTD) stations occupied from 21 February to 22 March, 58 stations were selected for the sampling of dissolved inorganic carbon (DIC) and alkalinity (Figure 1). A Neil Brown CTD equipped with a Beckman oxygen sensor was used, as well as a 24 bottles rosette with 12 L Niskin bottles for water sampling. Two CTD casts were performed at each station: a surface one with 24 bottles from 1350 m up to the surface, and a deep one from the bottom up to 1350 m. Hydrological and geochemical parameters used in this study were all measured directly onboard following WOCE protocols [*WOCE Operations Manual*, 1991]. Salinity was measured using a Guildline salinometer in a constant temperature laboratory, oxygen by an automatic Winkler potentiometric titration system and nutrients (total nitrate, silicate and phosphate) with two automatic Technicon analyzers. Total alkalinity (TA) and DIC were measured simultaneously by a potentiometric titration system. Certified reference materials (CRMs) with known TA and DIC concentrations were used as standards (batch 30, provided by A.G. Dickson, Scripps Institute of Oceanography). Samples were also collected with 100 mL Pyrex syringes directly on Niskin bottles to measure CFCs using a gas chromatograph technique [*Mantisi et al.*, 1991].
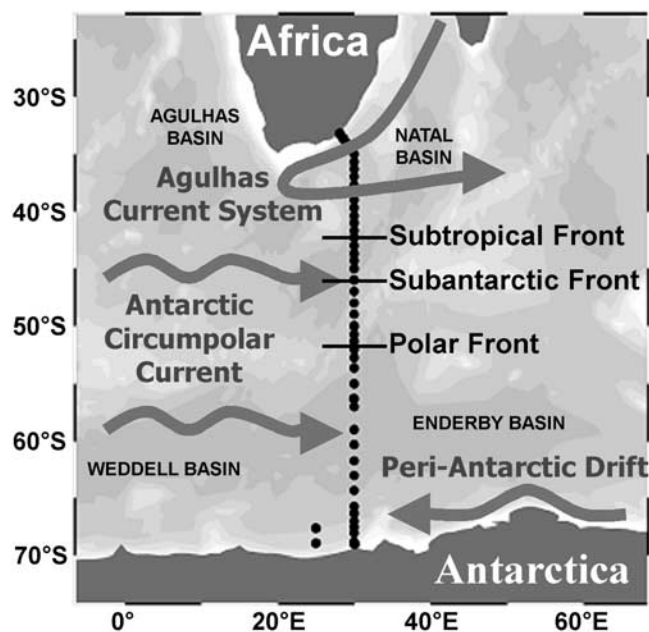

Figure 1. Map showing the location of stations visited during the Circulation et Ventilation dans l'Antarctique (CIVA)-2 cruise in February/March 1996 (World Ocean Circulation Experiment (WOCE) line I6). Only stations where dissolved inorganic carbon (DIC) and alkalinity data were collected are shown.

[6] Sampling protocols and measurement techniques followed during the cruise led to small errors: the standard deviation of the 45 deep replicate samples (3000 m) is ±0.3 µmol/kg for oxygen and ±1.9 µmol/kg for both alkalinity and DIC. The standard deviation calculated for CFC-11 is ±0.06 pmol/kg in deep replicate samples with low concentrations (<0.25 pmol/kg) and ±0.18 pmol/kg in replicate samples having higher CFC-11 concentrations. Errors associated with temperature and salinity measured with the CTD probe can be neglected in this study.

3. Hydrological Context

[7] From 33° to 70°S, the CIVA-2 cruise track crosses several hydrological fronts that separate the region into three main biogeochemical zones (Figure 1). Surface waters from the tropical Indian Ocean are transported southward by the Agulhas Current System, retroflecting south of Africa and flowing back to the Indian Ocean [e.g., *Gordon*, 2003]. The Subtropical Front is identified by the southern extension of the tropical warm and salty waters (42°S). Farther south, stand the subantarctic and Polar Front zones (42°–51°S). This frontal region is characterized by strong meridional gradients of all properties. The coldest and freshest waters are found in the Antarctic zone (51°–70°S), south of the Polar Front, flowing east in the Antarctic Circumpolar Current and west along the Antarctic coast in the Peri-Antarctic Drift. The deep ocean circulation is constrained by the Indian-Atlantic Ridge (~50°S) that separates the Agulhas-Natal Basin in the north from the Weddell-Enderby Basin in the south.

[8] Sections of salinity (S), dissolved inorganic carbon (DIC) and CFC-11 shown in Figure 2 reveal the main
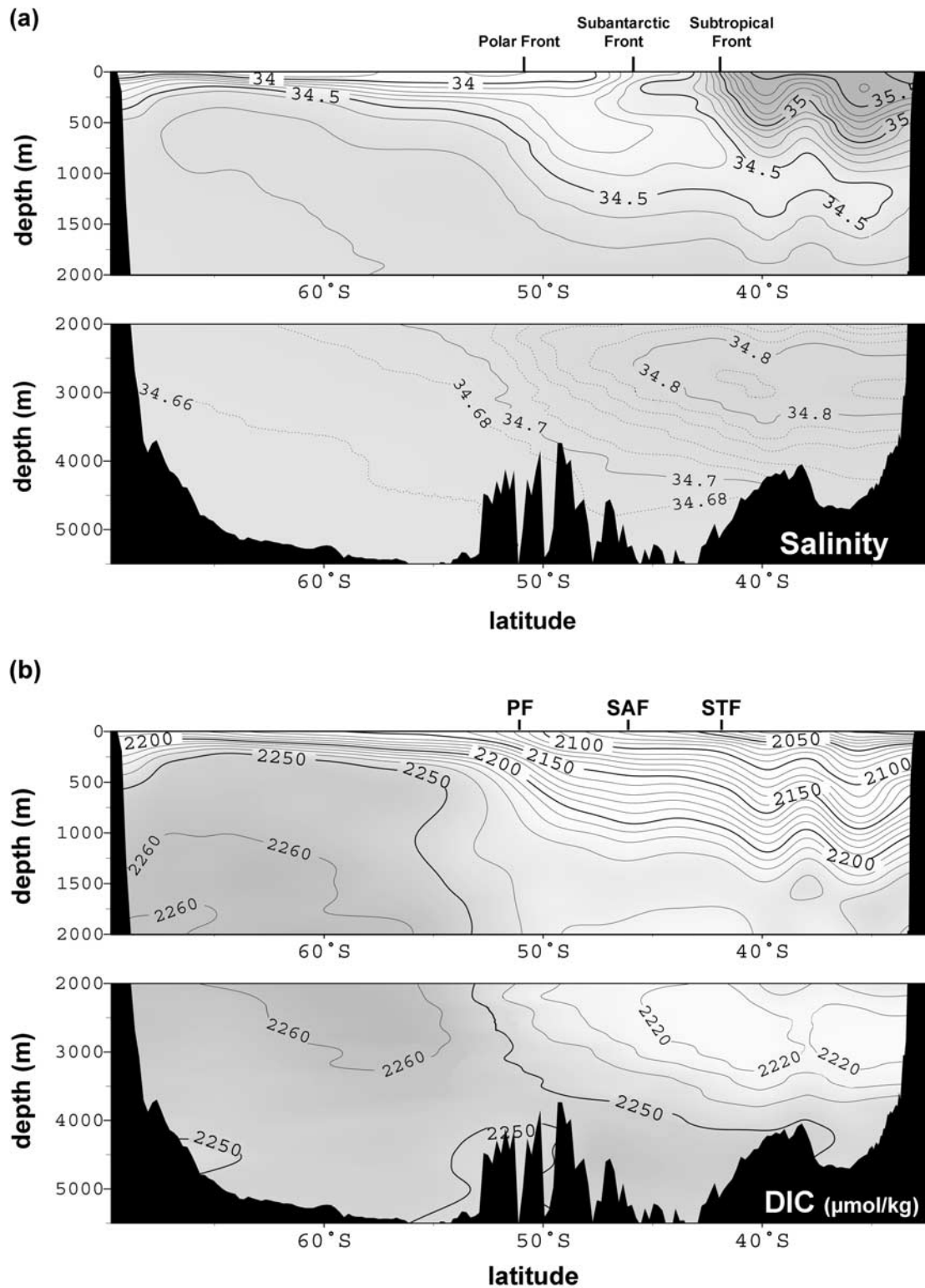
Figure 2. Vertical distributions of (a) salinity, (b) DIC (μmol/kg), and (c) CFC-11 (pmol/kg) along 30°E in the Southern Ocean (WOCE line I6).

features of the ocean circulation at the Indian-Atlantic boundary. In the subtropical zone, the distribution of all properties is governed by a deep meandering feature (down to 2000 m) generated by the Agulhas Return Current. In the frontal zone, the subduction of Antarctic Intermediate Water (AAIW) is well identify by the northward deepening of the salinity minimum down to 1500 m, together with the deepening of DIC and CFC-11 isolines. At greater depths,

Figure 2. (continued)

the salinity maximum ($S > 34.8$) associated with minimum concentrations in DIC (<2220 μmol/kg) and CFC-11 (<0.1 pmol/kg) is the signature of old North Atlantic Deep Water (NADW), which enters the Indian Ocean south of Africa [e.g., *Metzl et al.*, 1990; *Donohue and Toole*, 2003; *van Aken et al.*, 2004]. NADW is concentrated north of the Polar Front (51°S) around 3000 m 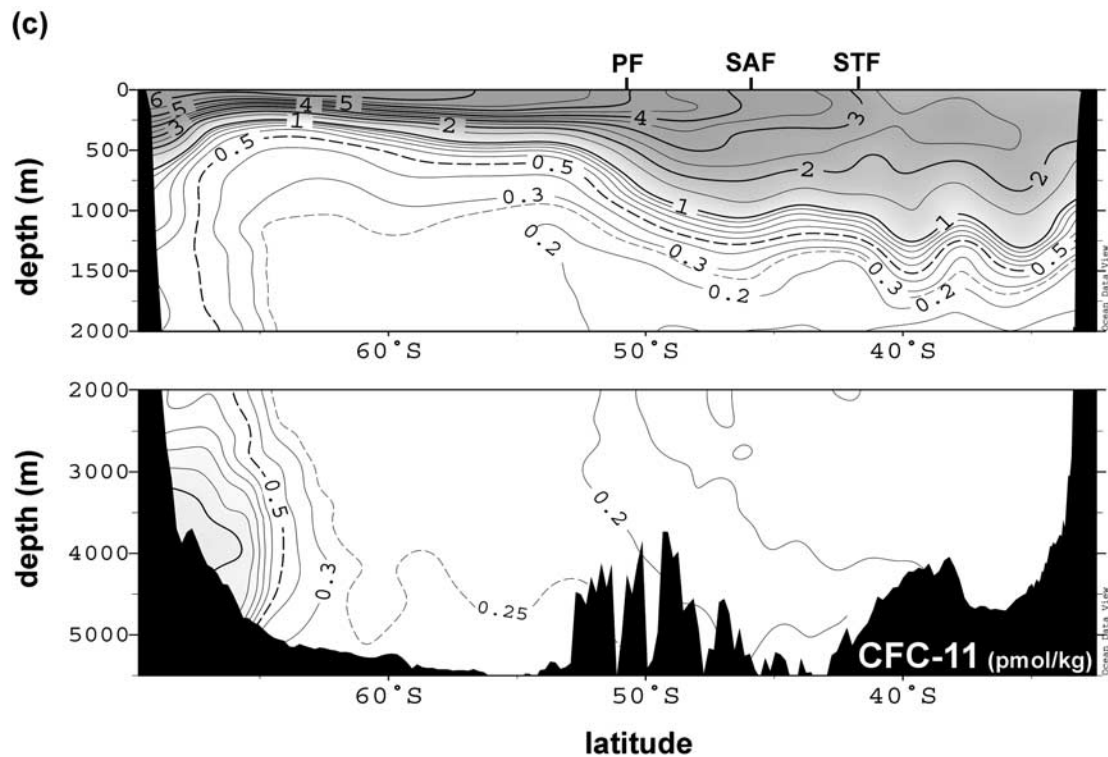depth. South of the Polar Front, the distribution of all properties is constrained by the large-scale upwelling circulation (Figure 2). Circumpolar Deep Water (CDW) is characterized by a maximum in DIC concentrations (2250–2270 μmol/kg) attributed to the influence of old waters from the Indian and Pacific Oceans [*Hoppema et al.*, 2000]. However, higher concentrations of CFC-11 measured in CDW (>0.2 pmol/kg) as compared to NADW also reveal the mixing with recently ventilated waters. Significant CFC-11 concentrations were also observed below 4000 m in the Agulhas-Natal basins (>0.2 pmol/kg) and Weddell-Enderby basins (>0.25 pmol/kg), as well as along the Antarctic slope (up to 1 pmol/kg). These cores of CFC-rich waters identify Antarctic Bottom Water (AABW) formed at several places around Antarctica [e.g., *Mantisi et al.*, 1991; *Archambeau et al.*, 1998; *Meredith et al.*, 2001; *Orsi et al.*, 2002].

[9] According to *Rintoul et al.* [2001], CDW is a composite of deep waters flowing from the Indian, Atlantic and Pacific basins that eventually mix with younger waters of local origin (e.g., Weddell Deep Water, Winter Water, Ice Shelf Water). This mixing produces recently ventilated waters (Modified-CDW) whose injection into middepth layers contributes to the ventilation of the deep Southern Ocean [*Orsi et al.*, 2002]. The formation process of AABW also involves Winter Water, Ice Shelf Water and deep waters of local origin such as Weddell Deep Water [e.g., *Gordon*, 1971; *Gill*, 1973; *Wong et al.*, 1998]. Relatively high levels

of CFCs measured in AABW indicate that this water was formed in the second half of the 20th century when CFCs were introduced in the atmosphere. In the 1950s, when CFCs started to increase in the atmosphere, the atmospheric CO₂ was already increased by 30 ppm (1/3 of the excess CO₂ observed today). As a consequence, one might expect the clear CFC signal detected along the Antarctic slope to be associated with a significant accumulation of anthropogenic CO₂.

4. Back-Calculation Technique

4.1. Formulation of Anthropogenic CO₂

4.1.1. Principle of the Method

[10] Anthropogenic CO₂ (C^{ant}) is separated from the "natural" DIC following the back-calculation technique described in *Körtzinger et al.* [1998]. This method is based on the calculation of the initial or preformed DIC concentration (C^0). When a water mass has been formed, it lost contact with the atmosphere with a preformed DIC concentration relative to the time of its formation ($C^{0,form}$). The amount of C^{ant} accumulated within this water mass is the difference between $C^{0,form}$ and the preindustrial preformed DIC ($C^{0,PI}$). Along their way to the ocean interior, water masses are supplied with DIC regenerated through biological processes (organic carbon remineralization and carbonate dissolution). Preformed DIC at the time of water mass formation ($C^{0,form}$) is estimated by removing the biological contribution (C^{bio}) from DIC concentrations measured in the water column ($C^{0,form} = C^m - C^{bio}$). The following formulation is obtained for C^{ant}:

$$C^{ant} = C^m - C^{bio} - C^{0,PI}. \qquad (1)$$

It is therefore possible to obtain C^{ant} from DIC measurements if we can estimate C^{bio} and $C^{0,\text{PI}}$.

4.1.2. Biological Contribution (C^{bio})

[11] According to *Brewer* [1978] and *Chen and Millero* [1979], the amount of carbon regenerated through organic carbon remineralization and carbonate dissolution can be deduced from the change in alkalinity (ΔTA) and oxygen (ΔO$_2$) by using the Redfield ratios, as follows:

$$C^{\text{bio}} = 0.5\Delta\text{TA} - \left(r_{\text{C/O}} + 0.5r_{\text{N/O}}\right)\Delta\text{O}_2. \qquad (2)$$

ΔTA is an increase in alkalinity defined as the difference between alkalinity measured in the water column and preformed alkalinity ($\Delta\text{TA} = \text{TA}^m - \text{TA}^0$). Apparent oxygen utilization (AOU) can be used for ΔO$_2$ in regions where surface oxygen is close to equilibrium with the atmosphere. AOU is the difference between oxygen saturation (calculated after *Benson and Krause* [1980]) and measured oxygen (AOU = O$_2^{\text{sat}}$ − O$_2^m$). In the Southern Ocean, however, the use of AOU is not a reliable concept since significant oxygen deficiencies were observed in surface waters in regions where ice coverage limits the air-sea exchange of oxygen [*Ito et al.*, 2004]. Instead, we prefer to use the true oxygen utilization (TOU) defined as the difference between preformed and measured oxygen (TOU = O$_2^0$ − O$_2^m$). In our study we used the ratios $r_{\text{C/O}} = 117/-170$ and $r_{\text{N/O}} = 16/-170$ given by *Anderson and Sarmiento* [1994], which are the most commonly used for estimating C^{bio} [e.g., *Gruber et al.*, 1996; *Sabine et al.*, 1999; *Ríos et al.*, 2003]. The coefficient assigned to TOU calculated from these ratios is 0.73, giving the following formulation:

$$C^{\text{bio}} = 0.5\left(\text{TA}^m - \text{TA}^0\right) + 0.73\left(\text{O}_2^0 - \text{O}_2^m\right). \qquad (3)$$

Parameterizations used for preformed alkalinity (TA^0) and preformed oxygen (O$_2^0$) are given in section 4.2.

4.1.3. Preindustrial Preformed Dissolved Inorganic Carbon (DIC) ($C^{0,\text{PI}}$)

[12] One way to estimate the preindustrial preformed DIC ($C^{0,\text{PI}}$) is to use a water mass formed before the industrial era as a reference. The preformed DIC calculated within this particular water mass ($[C^{0,\text{form}}]_{\text{REF}} = [C^m]_{\text{REF}} - [C^{\text{bio}}]_{\text{REF}}$) is an estimation of $C^{0,\text{PI}}$ in the formation region of the reference water. In order to estimate $C^{0,\text{PI}}$ in any region we must include a term accounting for regional differences (ΔC^0):

$$C^{0,\text{PI}} = [C^m]_{\text{REF}} - [C^{\text{bio}}]_{\text{REF}} + \Delta C^0. \qquad (4)$$

ΔC^0 is the difference between C^0 in any region and C^0 in the formation region of the reference water. We assume that this difference has remained constant since the preindustrial era and calculate ΔC^0 using the preformed DIC concentrations currently observed ($\Delta C^0 = C^{0,\text{obs}} - [C^{0,\text{obs}}]_{\text{REF}}$). The following formulation is obtained for $C^{0,\text{PI}}$:

$$C^{0,\text{PI}} = [C^m]_{\text{REF}} - [C^{\text{bio}}]_{\text{REF}} + C^{0,\text{obs}} - [C^{0,\text{obs}}]_{\text{REF}}. \qquad (5)$$

Combining equations (1) and (5) gives the following formulation for C^{ant}:

$$C^{\text{ant}} = C^m - C^{\text{bio}} - C^{0,\text{obs}} - \left([C^m]_{\text{REF}} - [C^{\text{bio}}]_{\text{REF}} - [C^{0,\text{obs}}]_{\text{REF}}\right). \qquad (6)$$

C^m is the DIC measured in the water column, C^{bio} is the regenerated DIC calculated from equation (3) and $C^{0,\text{obs}}$ is the contemporary preformed DIC estimated using parameterizations given in section 4.2.1. The other three terms constitute the reference ($\Delta C^{0,\text{REF}}$): $[C^m]_{\text{REF}}$ is the DIC measured in the reference water, $[C^{\text{bio}}]_{\text{REF}}$ is the regenerated DIC calculated in the reference water and $[C^{0,\text{obs}}]_{\text{REF}}$ is the preformed DIC currently observed in the formation region of the reference water. Calculation of the reference is detailed in section 4.2.3.

4.2. Parameterizations

4.2.1. Preformed DIC and Alkalinity

[13] Numerous parameterizations for preformed DIC and alkalinity are proposed in the literature. At a regional scale, surface DIC and alkalinity normalized to a constant salinity can be expressed as a function of the temperature only [e.g., *Poisson and Chen*, 1987; *Körtzinger et al.*, 1998; *Millero et al.*, 1998]. However, for large coverage data sets a better prediction is obtained when introducing other tracers such as salinity or nutrients [e.g., *Gruber et al.*, 1996; *Sabine et al.*, 1999; *Lee et al.*, 2000; *Ríos et al.*, 2003]. In this study, surface DIC and alkalinity are computed as a function of temperature (θ), salinity (S) and the conservative tracer PO [*Broecker*, 1974]. We used data collected after 1990 in the South Atlantic and south Indian Oceans during WOCE and Océan Indien Service d'Observation (OISO) cruises [*WOCE Data Products Committee*, 2002; *Jabaud-Jan et al.*, 2004; N. Metzl et al., Summer and winter air-sea CO$_2$ fluxes in the Southern Ocean, submitted to *Deep Sea Research*, 2004]. To avoid a potential systematic error in the predictions due to the seasonality of DIC and alkalinity [*Chen and Pytkowicz*, 1979], the data set was restricted to winter and early spring measurements since most water masses are formed during this period. The ratio O$_2$/P = −170 given by *Anderson and Sarmiento* [1994] is used to calculate PO (PO = O$_2$ − (−170) PO$_4$). Note that when phosphate data are not available PO is calculated from nitrate (PO = O$_2$ − (−170/16) NO$_3$). The following regressions were obtained in surface waters (0–50 m) for temperatures below 21°C (Figure 3):

$$C^{0,\text{obs}} = -0.0439\text{PO} + 42.790S - 12.019\theta + 739.83, \quad r^2 = 0.99 \qquad (7)$$

$$\text{TA}^0 = 0.0685\text{PO} + 59.787S - 1.448\theta + 217.15, \qquad r^2 = 0.96. \qquad (8)$$

The standard deviation of the prediction is ±6.3 μmol/kg for $C^{0,\text{obs}}$ ($n = 428$) and ±5.5 μmol/kg for TA^0 ($n = 243$). In the mixed layer DIC and alkalinity vary seasonally and equations (7) and (8) (winter relationships) should not be used to deduce preformed concentrations for summer. In the subantarctic zone the mixed layer can reach 500 m during winter, when mode waters are formed [*Metzl et al.*, 1999], but it is less than 200 m at higher latitudes [*Kara et al.*, 2003]. Consequently, we will disregard all estimates of $C^{0,\text{obs}}$ and TA^0 (and consequently C^{ant}) calculated above 500 m north of the Subantarctic Front (46°S) and above 200 m in the south.
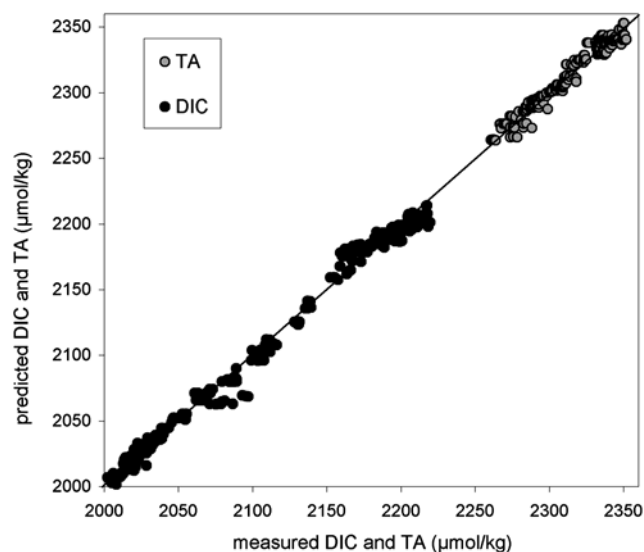
Figure 3. Plot of predicted DIC and alkalinity (TA) against measurements for winter and early spring in surface waters (0–50 m). Data are from the WOCE and Océan Indien Service d'Observation (OISO) cruises conducted in the South Atlantic and Indian Oceans. DIC and TA are predicted from regressions given in section 4.2.1 (equations (7) and (8)). The line is predicted = measured.

4.2.2. Preformed Oxygen

[14] In most regions of the world ocean surface oxygen concentration is close to equilibrium with the atmosphere at the time of water mass formation, usually in winter. In that case AOU can be used in the formulation of the biological contribution (equation (2)). In ice-covered region, the surface oxygen content can significantly deviate from equilibrium with the atmosphere due to the slow down of air-sea exchanges. In the Southern Ocean, a systematic oxygen undersaturation is observed in ice-covered surface waters due to the upwelling of deep waters depleted in oxygen. Consequently, the use of AOU for water masses formed in these particular regions (Antarctic deep and bottom waters) would result in an overestimation of the regenerated carbon (C^{bio}). Note that along the CIVA-2 transect, oxygen utilization ranges from about 50 to 150 μmol/kg, whereas ΔTA remains relatively low (<30 μmol/kg), suggesting that most of the regenerated carbon comes from respiration (Figure 4). The error made on C^{bio} (and consequently on C^{ant}) when inferred from AOU could be as large as 40 μmol/kg when oxygen depletion reaches 50 μmol/kg as reported by *Poisson and Chen* [1987] in the winter water of the Weddell Sea.

[15] In this study we performed two different calculations in order to evaluate the sensitivity of the back-calculation method to the degree of oxygen saturation in surface waters. First, we calculated C^{ant} assuming that surface waters are in equilibrium with the atmosphere ($O_2^0 = O_2^{sat}$). This result was then compared with the distribution of C^{ant} obtained when accounting for oxygen disequilibrium in ice-covered surface waters. For this purpose we used the following parameterization for preformed oxygen (O_2^0):

$$O_2^0 = O_2^{sat} - \alpha k O_2^{sat}, \qquad (9)$$

where k is the mixing ratio of ice-covered surface waters determined using a multiple end-member mixing model (model detailed in Appendix A) and α is the degree of
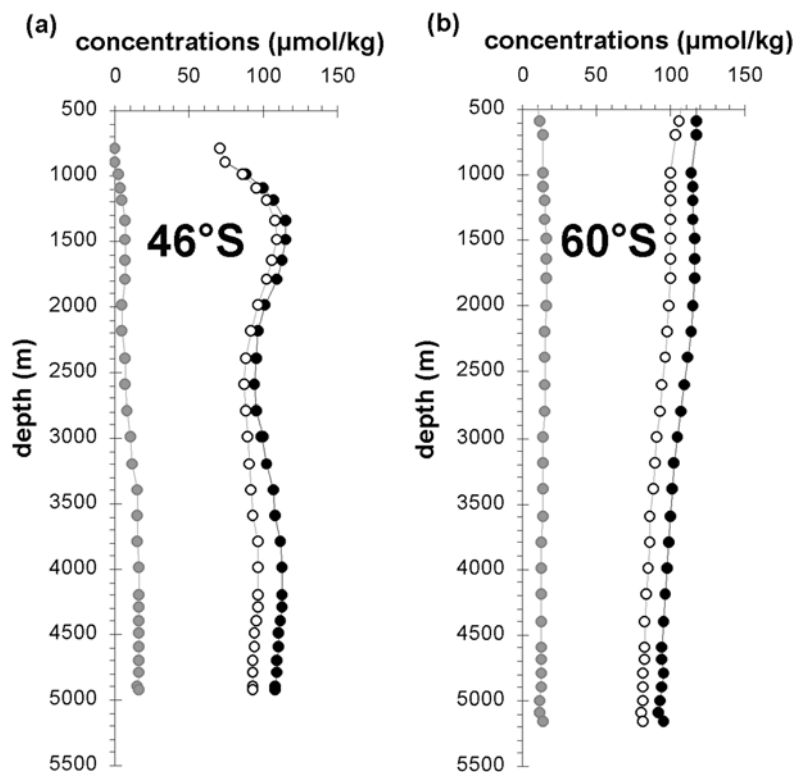

Figure 4. Examples of vertical profiles of C^{bio} (filled circles), 0.5 ΔTA (shaded circles), and 0.73 TOU (open circles) obtained along 30°E (a) in the subantarctic zone and (b) in the Antarctic zone.

oxygen undersaturation in ice-covered surface waters. In the first calculation, α is set equal to zero ($O_2^0 = O_2^{sat}$). In the second calculation, we chose the mean value $\alpha = 12\%$ calculated by *Anderson et al.* [1991] in ice shelf waters of the Weddell Sea. This number is in good agreement with the oxygen depletion observed by *Poisson and Chen* [1987] in the winter water (about 15%) as well as with observations collected farther east in Prydz Bay (70°E) by *Gibson and Trull* [1999] who reported between 10 and 20% oxygen undersaturation in surface waters covered with ice.

4.2.3. Reference Water

[16] The reference water, that contains a priori no anthropogenic CO$_2$, has to be an old water formed before the preindustrial era. In the Southern Hemisphere, the oldest waters are deep inflows originating from the Northern Hemisphere. These deep waters, which enter the Southern Ocean from the three main basins, should not have been in contact with the atmosphere since the beginning of the industrial era. We have chosen to take our reference in the North Atlantic Deep Water (NADW) that enters the Indian Ocean south of Africa. This choice is consistent with the distribution of C^{ant} obtained in the eastern South Atlantic by *Ríos et al.* [2003] showing C^{ant} concentrations below the detection limit in NADW.

[17] Along the CIVA-2 section, CFC-free cores of NADW were detected around 3000 m in the Agulhas-Natal Basin (Figure 2c). Calculation of the DIC regenerated within NADW ($[C^{bio}]_{REF}$) is based on the assumption that North Atlantic surface waters are in equilibrium with the atmosphere ($[O_2^0]_{REF} = [O_2^{sat}]_{REF}$). DIC and alkalinity regressions calculated from southern data (equations (7) and (8)) should not hold for NADW since it was formed in the North Atlantic. Instead, preformed DIC and alkalinity in NADW ($[C^{0,obs}]_{REF}$ and $[TA^0]_{REF}$) were predicted using regressions calculated from winter data collected north of 45°N in the North Atlantic [*WOCE Data Products Committee*, 2002]:

$$[C^{0,obs}]_{REF} = 70.325S - 10.725\theta - 270.63, \qquad r^2 = 0.76 \quad (10)$$

$$[TA^0]_{REF} = 36.9614S + 2.527\theta + 996.71, \qquad r^2 = 0.95. \quad (11)$$

The standard deviation of the prediction is ±9.1 μmol/kg for $C^{0,obs}$ ($n = 206$) and ±8.1 μmol/kg for TA^0 ($n = 55$). NADW was identified along the CIVA-2 section using the multiple end-member mixing model described in Appendix A: equations (10) and (11) were employed where the mixing ratio of eastern NADW exceed 50%.

[18] The reference ($\Delta C^{0,REF} = [C^m]_{REF} - [C^{bio}]_{REF} - [C^{0,obs}]_{REF}$) is calculated in the cores of NADW detected along the CIVA-2 section. We obtained a mean value of -51 ± 3 μmol/kg from the 76 samples where the mixing ratio of NADW exceed 50%. The absolute value of $\Delta C^{0,REF}$ correspond to the amount of C^{ant} accumulated in water masses that are currently formed in the North Atlantic. *Körtzinger et al.* [1998, 1999] calculated $\Delta C^{0,REF}$ in bottom waters originating from the Southern Hemisphere (AABW) in order to estimate C^{ant} in the North Atlantic. They

obtained a mean value of -62.7 μmol/kg for the latitude range 40°–50°N and -55 μmol/kg north of 50°N. These numbers can be compared with an estimation of the preformed DIC increase since the preindustrial era (ΔDIC) as deduced from the atmospheric pCO_2 increase (ΔpCO_2) with the use of the Revelle factor (R):

$$\Delta pCO_2/\Delta DIC = R(280\mu atm/2000\mu mol/kg), \qquad (12)$$

where 280 μatm and 2000 μmol/kg are the preindustrial values for pCO_2 and preformed DIC respectively [*Körtzinger et al.*, 1998]. Taking an atmospheric pCO_2 level of 360 μatm for the 1990s ($\Delta pCO_2 = 80$ μatm) and R ranging from 9 to 12, ΔDIC range between 47 and 64 μmol/kg. A mean value of 50 μmol/kg is obtained when using the mean Revelle factor 11.4 calculated from observations collected in the North Atlantic Ocean [*Takahashi et al.*, 1993]. These numbers compare well with the absolute value of $\Delta C^{0,REF}$ calculated for both NADW in the Southern Hemisphere and AABW in the North Atlantic.

4.3. Error Assessment

[19] All data-based methods currently used to estimate the storage of anthropogenic CO$_2$ in the ocean are based on a strong hypothesis about long-term ocean variability. Here we must assume that ocean dynamics, biological activity, as well as air-sea interactions do not change significantly on decadal to centennial timescales. Regional observations on multidecadal timescales have given some evidences that the ocean did not operate at a steady state, e.g., changes in salinity, temperature or oxygen [*Wong et al.*, 1999; *Levitus et al.*, 2000; *Andreev and Watanabe*, 2002; *Gille*, 2002; *Matear et al.*, 2000]. However, large uncertainties are still associated with the long-term variability of ocean processes and the error we make on C^{ant} estimates when assuming the steady state may not be significant if only small changes have occurred in the last centuries.

4.3.1. Systematic Errors

[20] The back-calculation technique described above is built on simplified biogeochemical concepts that can lead to potentially large errors on C^{ant} estimates. The error made on C^{bio} (and consequently on C^{ant}) when inferred from AOU could be large in Antarctic deep and bottom waters and it is therefore crucial to account for surface oxygen disequilibrium when resolving the distribution of C^{ant} in the Southern Ocean (see section 4.2.2.). A second source of systematic error in the formulation of C^{bio} (equation (2)) lies in the choice of the Redfield ratios. Several revised ratios are proposed in the literature [e.g., *Takahashi et al.*, 1985; *Anderson and Sarmiento*, 1994; *Körtzinger*, 2001]. The coefficient associated with oxygen utilization ranges from 0.73 to 0.86 when calculated from these different ratios. In this study we used the lower limit (0.73) calculated from the ratios given by *Anderson and Sarmiento* [1994]. However, using the upper limit (0.86) results in a maximum difference on C^{ant} estimates of 10 μmol/kg at intermediate depths (1500–2000 m) and less than 5 μmol/kg in deep and bottom waters [see also *Sabine and Feely*, 2001, Figure 6].

4.3.2. Random Errors

[21] The method is also subjected to random errors from measurements: DIC (±1.9 μmol/kg), TA (±1.9 μmol/kg) and

O_2 (± 0.3 μmol/kg) and from estimations of $C^{0,obs}$, TA^0, O_2^{sat} and $\Delta C^{0,REF}$. Errors associated with $C^{0,obs}$ and TA^0 are the standard deviations of the regressions in equations (7) and (8). The error assigned to O_2^{sat} (± 4.6 μmol/kg) was estimated by comparing O_2^{sat} estimates with oxygen measurements in the surface layer. Note that we excluded all samples collected south of 60°S (oxygen undersaturation α > 10%) because the issue of highly undersaturated waters is regarded as a potential systematic error. The standard deviation of $\Delta C^{0,REF}$ (± 3 μmol/kg) is used to estimate the random error. Note that $\Delta C^{0,REF}$ is also subjected to a potential systematic error due to the choice of the reference water (here NADW), but it cannot be estimated. The C/O_2 and N/O_2 ratios also are entitled to both random and systematic errors. Here we consider the random errors of ± 0.092 and ± 0.0081 obtained by propagating uncertainties given by *Anderson and Sarmiento* [1994].

[22] The overall random error associated with the calculation of C^{ant} was estimated following the method used by *Gruber et al.* [1996]. We calculated a statistical overall error on C^{ant} estimates ranging from 10 μmol/kg (in waters where oxygen utilization is low) to 17 μmol/kg (in waters where oxygen utilization is maximum). However, this range represents an upper limit. Using a model of random error propagation we estimated the mean uncertainty on C^{ant} estimates to range from 3 to 6 μmol/kg, depending on oxygen utilization. Because most anthropogenic CO_2 will be found in young waters where oxygen utilization is relatively low, it is reasonable to consider a mean uncertainty of 5 μmol/kg attached to random errors.

5. Results

5.1. Distribution of Anthropogenic CO₂

[23] Two calculations are performed in order to highlight the uncertainty associated with estimates of oxygen utilization. In the first calculation, surface waters are assumed to be in equilibrium with the atmosphere (α = 0 in equation (9)). The distribution of C^{ant} obtained along 30°E is presented in Figure 5a. Strong vertical gradients of C^{ant} are observed in subsurface and intermediate waters where concentrations range from 10 to 60 μmol/kg. North of the Subtropical Front (42°S) the distribution of C^{ant} follows the eddy and meandering structures generated by the Agulhas Return Current down to 2000 m. The deepest penetration of C^{ant} occurs around 35°–40°S and is associated with the spreading of intermediate and mode waters. South of the Polar Front (51°S), the penetration of C^{ant} is shallow likely because of a strong stratification of the water column due to the presence of the winter layer and the upwelling of old deep waters. Minimum concentrations of C^{ant} are found in deep waters, with values below the detection limit in NADW and between 5 and 10 μmol/kg in CDW. In AABW, concentrations of C^{ant} are higher than in the overlying deep waters. North of the Indian-Atlantic Ridge, C^{ant} concentrations in bottom waters are low (5–6 μmol/kg). South of the ridge, two cores with high C^{ant} concentrations are detected in agreement with CFC data. One core localized between 55°S and 60°S (8–10 μmol/kg) would originate from the Weddell Sea, while the other one, detected around 3000 m along the continental slope (10–12 μmol/kg), would correspond to AABW formed east

of the section, probably in Prydz Bay [*Schodlok et al.*, 2001].

[24] As discussed before, deep and bottom layers of the Southern Ocean are ventilated through the spreading of dense waters formed at several places around Antarctica, in region where surface oxygen concentrations are well below the saturation level due to ice coverage. When assuming oxygen equilibrium in surface waters we overestimate the oxygen utilization in CDW and AABW, and consequently underestimate C^{ant} concentrations. In the second calculation, we assume a mean oxygen undersaturation α = 12% in surface waters covered with ice (equation (9)). The new estimates of C^{ant} are presented in Figure 5b. North of 50°S estimates of C^{ant} are similar, except in AABW (below 4000 m) where C^{ant} concentrations are higher in the second calculation. The correction decreases C^{bio} (by decreasing oxygen utilization) in water masses ventilated from the south, leading to higher C^{ant} concentrations: in CDW and AABW, corrected estimates of C^{ant} are two to three times higher than in the initial calculation.

5.2. Comparison With CFCs

[25] Although transient tracers are not used in the back-calculation method described above, a good agreement is obtained between the distribution of CFC-11 (Figure 2c) and the distribution of C^{ant} (Figure 5). In the subtropical/subantarctic region, a deep penetration of CFC-11 and C^{ant} occurs down to 2000 m, whereas south of 50°S the strong stratification of the water column limits the tracers penetration. High C^{ant} concentrations estimated in CDW and AABW are supported by significant CFC-11 concentrations (>0.2 pmol/kg) which undoubtedly reveal the mixing with recently ventilated waters. Particularly high concentrations of CFC-11 were measured in AABW flowing along the Antarctic slope (>1 pmol/kg), where estimates of C^{ant} are up to 25 μmol/kg (Figure 5b). However, in the core of AABW originating from the Weddell Sea, slightly lower values of C^{ant} (22–23 μmol/kg) are associated with much lower CFC-11 concentrations (0.25–0.3 pmol/kg).

[26] We investigate further the similarities and differences observed between CFC-11 data and C^{ant} estimates by focusing on Antarctic Intermediate Water (AAIW) and AABW (Figure 6). These two water masses formed in the Southern Ocean are young enough to carry a significant amount of both tracers. In the salinity minimum layer which characterizes AAIW, two different relationships are found (Figure 6a). In the frontal region, the C^{ant}/CFC-11 relationship is very close to that reported by *Ríos et al.* [2003] using data collected in the eastern South Atlantic (WOCE line A14, 1995). In the Agulhas Current region, the slope of the regression line is higher, which probably reflects both an increased uptake of C^{ant} with higher surface temperature (Revelle factor) and mixing with surrounding waters. Two different trends in the C^{ant}/CFC-11 relationship are also found in AABW (Figure 6b). The slope of the regression line is lower when approaching the Antarctic slope, in AABW originating mainly from the eastern side of the section (e.g., Prydz Bay). By comparing the atmospheric histories of CFC-11 and CO_2 we expect that the theoretical C^{ant}/CFC-11 relationship showed a decrease in the slope of the regression line from the middle of the 20th century to the 1980s. This suggests that AABW detected along the Ant-
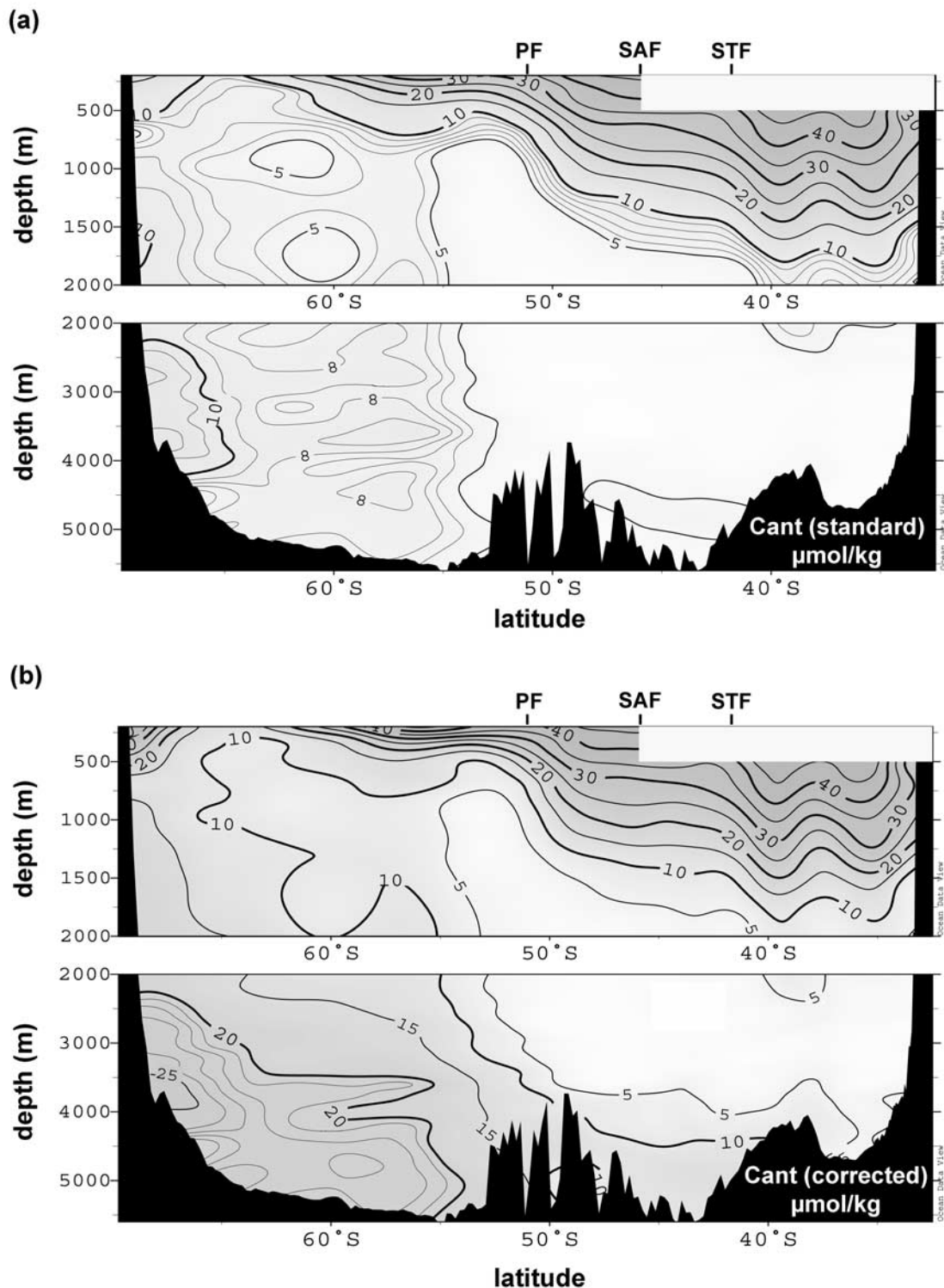
Figure 5. Distribution of anthropogenic CO_2 (C^{ant} in μmol/kg) estimated along 30°E in the Southern Ocean (WOCE line I6, 1996). C^{ant} estimates are obtained using the back-calculation technique described by *Körtzinger et al.* [1998]. In Figure 5a we assume that surface oxygen is in equilibrium with the atmosphere ($\alpha = 0$). Corrected estimates of C^{ant} in Figure 5b are obtained by accounting for oxygen undersaturation in surface waters covered with ice ($\alpha = 12\%$).

Figure 6. Relationships obtained between measured CFC-11 and C^{ant} estimates along 30°E (WOCE line I6, 1996). (a) Data from the salinity minimum layer, which characterizes Antarctic Intermediate Water (AAIW) ($S < 34.5$). Relationships observed in the Agulhas Current region (open circles) and in the frontal region (shaded circles) are compared with the relationship obtained by *Ríos et al.* [2003] in the eastern South Atlantic (thin line). (b) data from Antarctic Bottom Water (AABW) detected below 4000 m in the Agulhas-Natal and Weddell-Enderby basins ($\sigma_\theta > 27.86$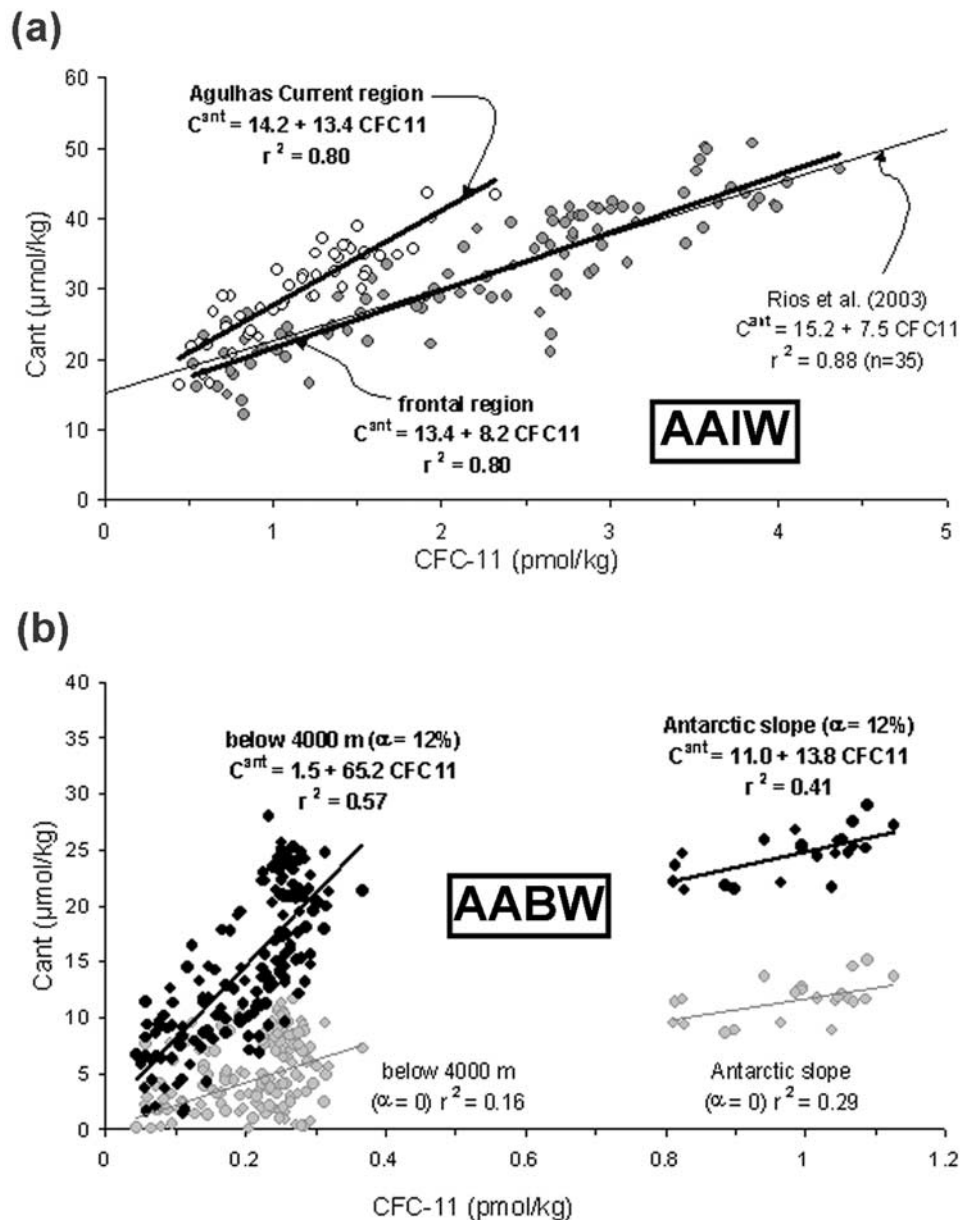) and along the Antarctic slope (deep CFC-11 >0.8 pmol/kg). Shaded circles show the relationships obtained when assuming surface oxygen equilibrium ($\alpha = 0$). Filled circles show the relationships obtained when accounting for 12% oxygen undersaturation in ice-covered surface waters.

arctic slope could be younger than AABW of Weddell Sea origin found north of 65°S. In Figure 6b, we also compared the C^{ant}/CFC-11 relationships obtained with the two different calculations. It is interesting to note that relationships are rather poor when assuming oxygen equilibrium in surface waters. A much better correlation is obtained between the two tracers when accounting for oxygen disequilibrium in

ice-covered surface waters and we believe that C^{ant} estimates are more robust in that latter calculation.

5.3. Anthropogenic CO$_2$ Inventories

[27] Corrected estimates of C^{ant} presented in Figure 5b were used to evaluate C^{ant} inventories along 30°E in the Southern Ocean (Figure 7). Inventories were calculated at
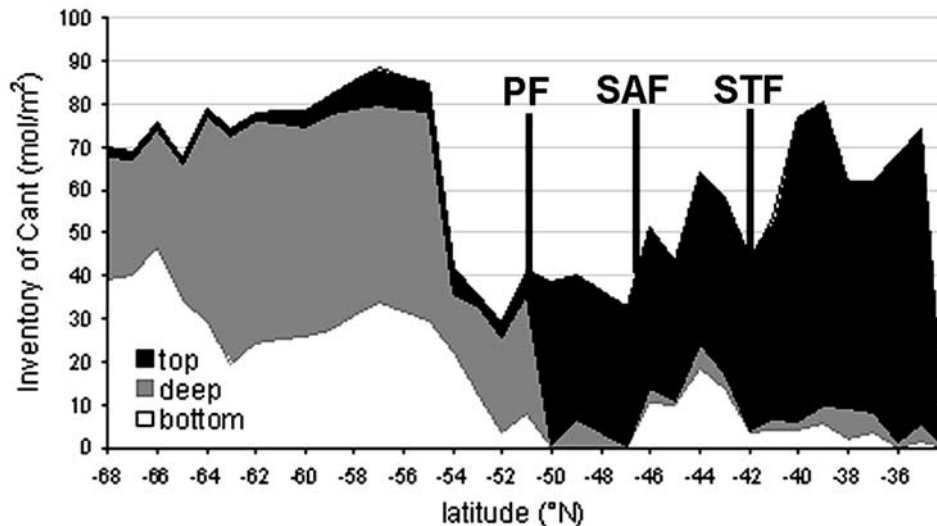
Figure 7. Inventories of C^{ant} obtained along 30°E when accounting for oxygen undersaturation in ice-covered surface waters (WOCE line I6, 1996). The water column is partitioned into three layers: a top layer, including surface, mode, and intermediate waters ($\sigma_\theta < 27.7$), a deep layer down to about 4000 m ($\sigma_\theta = 27.7$–27.86), and a bottom layer ($\sigma_\theta > 27.86$), also including the high-CFC waters detected along the Antarctic slope (deep CFC-11 > 0.8 pmol/kg).

each station by integrating C^{ant} concentrations from the surface down to the bottom (column inventories). In the surface layer, where the back-calculation technique is not reliable, we assumed constant C^{ant} concentrations and the value calculated at the bottom of the mixed layer (500 m north of 46°S and 200 m in the south) was extended up to the surface, which introduced a potential bias in surface estimates of C^{ant}. However, C^{ant} concentrations should be rather homogeneous in the mixed layer at least during winter and the mean error should not exceed 10 μmol/kg. Integrating this error over 200–500 m results in a relatively small uncertainty on C^{ant} inventories: about 5 mol/m² north of 46°S and 2 mol/m² in the south, which represents less than 10% of the column inventories calculated in these regions.

[28] In order to evaluate the relative contribution of top, deep and bottom waters to the column inventory the water column is partitioned into three layers (Figure 7). North of 50°S, the storage of C^{ant} essentially occurs in mode and intermediate waters ($\sigma_\theta < 27.7$). In the Agulhas Current region, column inventories range from 60 to 80 mol/m². The maximum value of 80 mol/m² is found where the 27.7 isopycnal deepens down to 2000 m. In the frontal region, inventories of C^{ant} decrease down to 30–50 mol/m², except between 42° and 46°S where a significant storage of C^{ant} also occurs in bottom waters (about 1/5 of the column inventory). South of the Polar Front (51°S), the water volume in the top layer is considerably reduced in the favor of upwelled deep waters. The contribution of the top layer to the column inventories almost drops to zero south of 51°S while the storage of C^{ant} in the deep layer rapidly increases up to 50 mol/m². This sudden raise in the contribution of deep waters results from both a larger water volume and the influence of recently ventilated waters with high concentrations of C^{ant}. Note the good agreement between the increase in C^{ant} inventories occurring between 52°S and 54°S and the 0.2 pmol/kg isoline in the

distribution of CFC-11 near 53°S (Figure 2c). The storage of C^{ant} in bottom waters also increases rapidly between 52°S and 54°S to reach the mean value of 30 mol/m² in the latitude range 55°–65°S. At these latitudes, the storage of C^{ant} in bottom waters is lower than in the overlying deep waters (about one third of the column inventory against more than half in the deep layer). In contrast, when approaching the Antarctic continent, the storage of C^{ant} decreases down to about 30 mol/m² in the deep layer (due to the lower water volume) while it increases up to 40–45 mol/m² in the bottom layer (due to high C^{ant} concentrations along the slope). As a consequence, the column inventory of C^{ant} remains high and relatively constant throughout all the Antarctic zone (70–90 mol/m²).

[29] Inventories of C^{ant} were also calculated using the initial distribution of C^{ant} obtained when assuming oxygen equilibrium ($\alpha = 0$) and compared with inventories described above ($\alpha = 12\%$) in Table 1. Correction of oxygen utilization only has an impact on water masses ventilated from the south ($k > 0$ in equation (9)). Consequently, inventories of C^{ant} are similar north of 50°S, except between 42 and 46°S where no significant storage of C^{ant} was found in the bottom layer when assuming oxygen equilibrium. South of 50°S, the correction has a dramatic impact on C^{ant} inventories: when assuming a mean oxygen undersaturation of 12% in surface waters covered with ice C^{ant} inventories increase by a factor of 1.5 to 2 in the deep layer and by a factor of 2 to 3 in the bottom layer. This results in a doubling of the mean column inventory south of 50°S.

[30] *Gruber et al.* [1996] estimated the error on the total inventory to be about 20%, based on a signal-to-noise ratio of 10/50 for C^{ant} estimates. In this study, we estimated the error associated with C^{ant} concentrations to be about 5 μmol/kg and maximum concentrations up to 50 μmol/kg in subsurface waters, giving a signal-to-noise ratio of 10% for C^{ant} estimates. This translates into a maximum error of 9 mol/m² on C^{ant} inventories calculated in this region. When

Table 1. Mean Inventories of C^{ant} Estimated Along 30°E in the Southern Ocean (WOCE line I6, 1996) Using Two Different Methods (C^0 and ΔC^* Methods)[a]

	C^0 Method		ΔC^* Method	
	$\alpha = 0$	$\alpha = 12\%$	$\alpha = 0$	$\alpha = 12\%$
Agulhas Current Region (34°–40°S)				
Top layer	64	64	42	42
Deep layer	<5	<5	<5	<5
Bottom layer	<5	<5	<5	<5
Total	**68**	**70**	**44**	**46**
Subantarctic Zone (42°–46°S)				
Top layer	38	38	20	20
Deep layer	<5	<5	<5	<5
Bottom layer	<5	11	<5	7
Total	**43**	**52**	**22**	**29**
Polar Front Zone (47°–51°S)				
Top layer	27	28	11	12
Deep layer	<5	8	<5	5
Bottom layer	<5	<5	<5	<5
Total	**29**	**38**	**12**	**18**
Weddell-Enderby Basin (55°–64°S)				
Top layer	<5	<5	<5	<5
Deep layer	27	49	17	39
Bottom layer	10	28	6	23
Total	**40**	**80**	**25**	**65**
Antarctic Slope (South of 65°S)				
Top layer	<5	<5	<5	<5
Deep layer	16	29	11	24
Bottom layer	18	40	12	33
Total	**35**	**70**	**24**	**58**

[a]C^{ant} inventories are in mol/m^2. Two calculations are performed for each method. In the first calculation we assume that surface oxygen is in equilibrium with the atmosphere ($\alpha = 0$). In the second calculation a mean oxygen undersaturation $\alpha = 12\%$ was assumed in surface waters covered with ice. The water column is separated into three layers (top, deep, and bottom) using criteria given in Figure 7.

the uncertainty attached to C^{ant} inventories calculated in the surface layer is added (2–5 mol/m^2), we obtain maximum errors <13 mol/m^2 north of 46°S and <11 mol/m^2 in the frontal and Antarctic regions.

6. Discussion

[31] North of the Polar Front, the most prominent feature is the deepening of C^{ant} isolines around 40°S which was also identified in the Atlantic, Indian and Pacific sectors from both data-based methods and models [e.g., *Gruber*, 1998; *Sabine et al.*, 1999; *Orr et al.*, 2001; *Sabine et al.*, 2002]. The persistency of this structure with time, as well as its large spreading around Antarctica suggest that the process of intermediate and mode waters formation occurring in the frontal zone would play an important role in the pumping and transport of anthropogenic CO$_2$: C^{ant} enters the Southern Ocean in the frontal region and is transported northward along isopycnal surfaces. Such dynamics explain the shift observed between maximum uptake of C^{ant} at high latitudes [*Takahashi et al.*, 2002] and maximum storage of C^{ant} in midlatitude regions where intermediate and mode waters converge [e.g., *Caldeira and Duffy*, 2000; *Orr et al.*, 2001; *Wallace*, 2001a].

[32] In the Antarctic zone, estimates of C^{ant} obtained in this study indicate that the entire water column has already

been invaded, suggesting that processes of dense water formation occurring around Antarctica are a major pathway for C^{ant} to penetrate deeply into the ocean interior. However, although this result is consistent with CFC-11 data collected around Antarctica (Figure 2c) [e.g., *Orsi et al.*, 2002], contradictory results were obtained in previous data-based studies [e.g., *Poisson and Chen*, 1987; *Sabine et al.*, 1999]. *Poisson and Chen* [1987] reported low estimates of C^{ant} in bottom waters flowing out of the Weddell Sea (6 µmol/kg in 1981), whereas we obtained about 10 µmol/kg in AABW originating from the Weddell Sea. These two results were obtained using the same biogeochemical concepts, but a major difference lies in the choice of the reference: in the calculation made by *Poisson and Chen* [1987] it is assumed that deep waters of the Weddell Sea are free from anthropogenic CO$_2$, which is in contradiction with the distribution of CFCs observed during the 1980s in this region [*Meredith et al.*, 2001]. This choice probably led the authors to underestimate C^{ant} concentrations in Weddell Sea Bottom Water. *Sabine et al.* [1999] used the ΔC^* method developed by *Gruber et al.* [1996] to estimate C^{ant} concentrations in the Indian Ocean, including the southwestern region investigated here. The distribution of C^{ant} obtained with this method also exhibits a maximum storage between 30° and 40°S, but the magnitude of their estimates is systematically lower than ours. In deep and bottom waters, the ΔC^* method did not permit to estimate a significant increase in C^{ant} concentration, leading the authors to conclude that C^{ant} concentrations should not exceed 10 µmol/kg in the deep Southern Ocean. *Wanninkhof et al.* [1999] undertook a comparative study of different data-based methods in the North Atlantic Ocean by comparing C^{ant} estimates with CFC data. Their results show that the ΔC^* method also failed in reproducing the deep penetration of C^{ant} in the North Atlantic, leading to the conclusion that this method may underestimate the penetration of C^{ant} in high latitude regions where dense water masses are formed. Using the initial back-calculation method (thereafter C^0 method), *Körtzinger et al.* [1998] estimated significant concentrations of C^{ant} down to the bottom in the North Atlantic Ocean, in accordance with CFC data. It then appears that the C^0 method may be more adapted to high latitudes regions as compared to the ΔC^* method.

[33] In order to compare the two approaches along the same line, we applied the ΔC^* method to the CIVA-2 data set using the same parameterizations as by *Sabine et al.* [1999]. As for the C^0 method, two calculations were performed using either AOU or TOU to predict oxygen utilization. The difference in C^{ant} estimates obtained with the C^0 and ΔC^* methods is shown in Figure 8 (note that these differences remain the same whether AOU is corrected or not). Concentrations of C^{ant} obtained with the ΔC^* method are lower everywhere along the section. The maximum difference (20 µmol/kg) is found around 1500 m, just below the salinity minimum layer. A better agreement is obtained in the core of the salinity minimum layer (AAIW) where estimates of C^{ant} are less than 10 µmol/kg lower with the ΔC^* method. In deep waters, the two methods lead to very similar results. Surprisingly, the difference in C^{ant} estimated in AABW is also small (between 4 and 6 µmol/kg). This implies that *Sabine et al.* [1999] would have detected a significant accumulation of C^{ant} in AABW
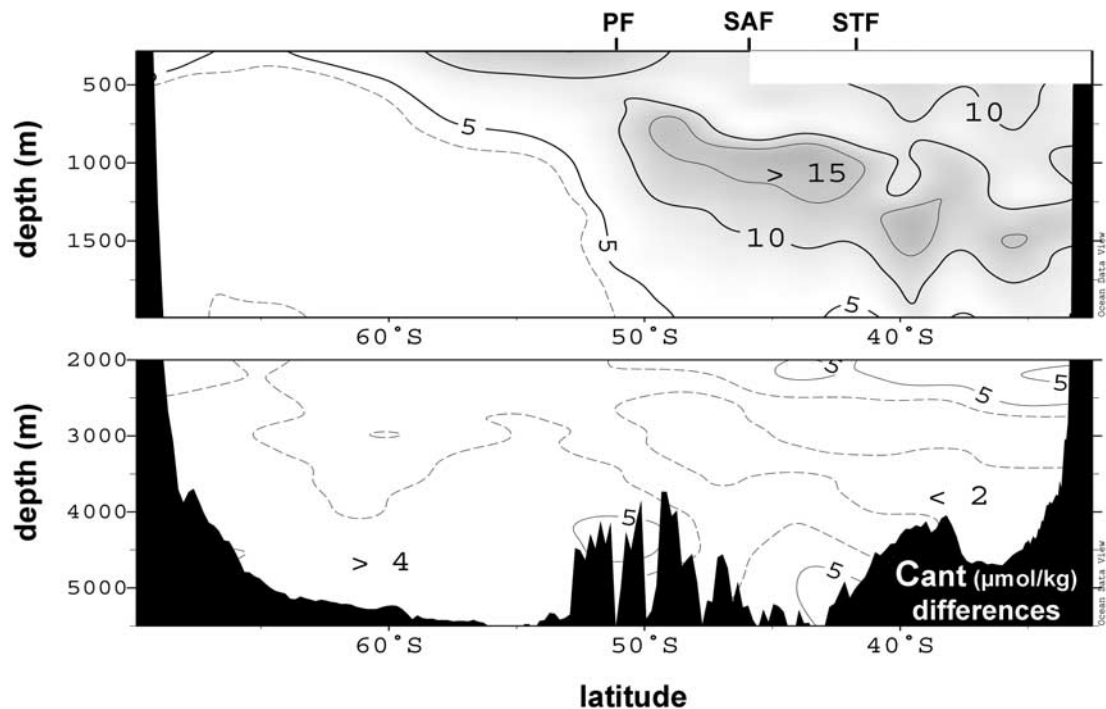
Figure 8. Differences of C^{ant} (μmol/kg) estimated using the C^0 method and the ΔC^* method along 30°E in the Southern Ocean (WOCE line I6, 1996).

if they had used TOU instead of AOU in the formulation of regenerated DIC. The mean inventories of C^{ant} obtained with the ΔC^* method using either AOU (α = 0) or TOU (α = 12%) are compared in Table 1. As expected from Figure 8, column inventories are lower with the ΔC^* method than with the C^0 method (about 10 mol/m^2 lower in the south and 20 mol/m^2 lower in the north). It is also interesting to note that when using TOU instead of AOU column inventories of C^{ant} increase by about 20 mol/m^2 for both methods.

[34] The ΔC^* method is also based on equation (1) (back-calculation technique). The biological contribution (equation (2)) is estimated in the same manner by both methods, except for the parameterization of preformed alkalinity (see TA^0 parameterization by *Sabine et al.* [1999]). However the two different parameterizations used for alkalinity lead to very similar results (differences in TA^0 < 6 μmol/kg). Instead, differences in C^{ant} concentrations are attributed to the way $C^{0,PI}$ is estimated. In the ΔC^* approach, $C^{0,PI}$ is derived from the knowledge of the atmospheric history of CO$_2$ and water mass ages: $C^{0,PI}$ is the DIC concentration the water would have in equilibrium with a preindustrial atmosphere (pCO_2 = 280 μatm) corrected for the fact that CO$_2$ in surface waters is rarely in full equilibrium with the atmosphere. The disequilibrium term (ΔC^{dis}) is determined along isopycnal surfaces by using transient tracers to obtain information on the time of water mass formation (water mass age). In *Sabine et al.* [1999], water mass ages were derived from CFC-12. The limitation of using CFCs as an analog for C^{ant} has been discussed by numerous authors [e.g., *Wallace et al.*, 1994; *Broecker*, 2001; *Thomas and England*, 2002; *Matear et al.*, 2003]. Here, the main problem with the CFCs age method concerns water masses of intermediate age, i.e., water masses older than 40 years for which the CFCs age method is not straightforward, but

young enough to carry a substantial amount of CFCs, and consequently C^{ant} [*Sabine et al.*, 1999]. These waters lie just below the salinity minimum layer (σ$_\theta$ = 27.3–27.5) where we found the largest difference between the ΔC^* and C^0 methods (Figure 8). According to *Sabine et al.* [1999, p. 187], in these particular waters "the effect of using the ΔC^* technique in waters that actually have anthropogenic CO$_2$ would be to overestimate the disequilibrium term and thus underestimate the anthropogenic CO$_2$." This implies that the maximum penetration depth of C^{ant} obtained with the ΔC^* method is probably too shallow (about 1500 m in the Agulhas Current region). This is in good agreement with results obtained from the C^0 method (penetration down to 2000 m). The other problem with the disequilibrium term (ΔC^{dis}) is that it is set to a constant value of −18.6 μmol/kg along deep isopycnal surfaces (σ$_\theta$ > 27.8). This mean value was estimated in waters where CFCs are below the detection limit, assuming that these waters are also free from anthropogenic CO$_2$ [*Sabine et al.*, 1999]. However, given that anthropogenic CO$_2$ was introduced in the atmosphere well before CFCs, this hypothesis may have led to overestimate the mean disequilibrium and, consequently, underestimate C^{ant} in Antarctic deep and bottom waters.

[35] *Holfort et al.* [1998] proposed a modification of the ΔC^* method, using CCl$_4$ rather than CFCs in the calculation of air-sea CO$_2$ disequilibrium (see review by *Wallace* [2001b]). One of the advantages of using CCl$_4$ is that it was introduced in the atmosphere at the beginning of the 20th century and has therefore penetrated slightly deeper in the water column than CFCs [*Wallace et al.*, 1994]. C^{ant} estimates obtained by *Holfort et al.* [1998] in the South Atlantic Ocean using CCl$_4$ are about 5–15 μmol/kg higher than C^{ant} estimates obtained by *Gruber* [1998] in the same

region using CFCs. Comparison of the vertical profile of C^{ant} also shows that when using CCl_4 rather than CFCs, the penetration of C^{ant} is about 500 m deeper around 30°S (down to 2000 m). These results are consistent with our findings. The ΔC^* method has been further improved in recent studies [e.g., *Pérez et al.*, 2002; *Sabine et al.*, 2002]. Along the WOCE line SR3 at the Indian-Pacific boundary (145°E), *Sabine et al.* [2002] obtained a deep penetration of C^{ant} at midlatitudes (1500–2000 m) and significant C^{ant} concentrations along the Antarctic slope (>10 μmol/kg). This result is in good agreement with the study published by *McNeil et al.* [2001] who used a multivariate approach (multiparametric linear regression (MLR) method [*Wallace and Johnson*, 1994]) to compare observations collected in 1968 and 1996 at the Indian-Pacific boundary. They found that C^{ant} had increased by 13 ± 10 μmol/kg along the Antarctic slope over this 28 year period.

[36] In the Southern Ocean, large disagreements are found between inventories of C^{ant} calculated from current global ocean models. In the framework of the Ocean Carbon Model Intercomparison Project for example (OCMIP [*Orr et al.*, 2001]), inventories of C^{ant} calculated in the South Atlantic Ocean from four different models are higher in midlatitude than in high latitude regions: model inventories range from 15 to 50 mol/m² in the band 30°–50°S and from 10 to 45 mol/m² south of 50°S. Our results, together with previous data-based studies also show high inventories in the subtropical/subantarctic band: 20–70 mol/m² at the Indian-Atlantic boundary (this study), 20–40 mol/m² in the Indian sector [*Sabine et al.*, 1999] and up to 50 mol/m² and 65 mol/m² in the Atlantic sector (*Gruber* [1998] and *Ríos et al.* [2003], respectively). In the Antarctic zone (south of 50°S), model results are within the range of data-based inventories obtained from the initial C^0 and ΔC^* methods: from 25 to 40 mol/m² along 30°E (this study), around 10 mol/m² in the Indian Ocean [*Sabine et al.*, 1999] and <20 mol/m² in the Atlantic Ocean [*Gruber*, 1998]. However, when both the C^0 and ΔC^* methods are corrected for oxygen undersaturation, C^{ant} inventories became much higher (from 58 to 80 mol/m²), suggesting that all four OCMIP models underestimate the storage of C^{ant} in the Southern Ocean.

7. Summary and Conclusions

[37] The distribution of anthropogenic CO_2 (C^{ant}) was estimated along 30°E in the Southern Ocean using the preformed DIC (C^0) method, a back-calculation technique previously used in the North Atlantic Ocean by *Körtzinger et al.* [1998]. A first calculation was performed by assuming that surface oxygen is in equilibrium with the atmosphere. In the second calculation, the oxygen utilization was corrected in order to take into consideration the large oxygen disequilibrium observed in surface waters covered with ice. These two results are then compared with C^{ant} estimated using the ΔC^* method, a back-calculation technique developed by *Gruber et al.* [1996]. North of 50°S, both methods agree on a deep penetration of C^{ant} around 40°S associated with the formation and spreading of intermediate and mode waters. The distribution of C^{ant} obtained in this midlatitude region is in good agreement with C^{ant} estimates in the south Indian, Atlantic, and Pacific

Oceans (data-based methods and models). South of 50°S, significant C^{ant} concentrations were detected in Antarctic deep and bottom waters with both the C^0 and ΔC^* methods (>5 μmol/kg). This result differs from previous data-based estimates of C^{ant} obtained in the Atlantic and Indian Ocean, but is in good agreement with CFC measurements.

[38] Evidences have been given that deep and bottom waters of the Southern Ocean are supplied with CFCs (and consequently C^{ant}) through mixing processes associated with the formation of dense water masses (Modified-CDW and AABW). As pointed out by *Chen* [2001, p. 29], "the sinking of the dense cold water, undetected by *Sabine et al.* [1999], represents a unique process and should not be overlooked." We reevaluated inventories of C^{ant} along 30°E and found that the contribution of M-CDW and AABW significantly raises the column inventories south of 50°S, with high-latitude waters storing as many C^{ant} as midlatitude waters. When oxygen disequilibrium in ice-covered surface waters is taken into consideration, column inventories double in Antarctic waters and the storage of C^{ant} becomes higher at high latitudes than at midlatitudes. This finding is opposed to what is usually obtained by ocean models. As a consequence, if the feature we obtained along 30°E is representative of other areas in the Southern Ocean, the global ocean budget of anthropogenic carbon could be much larger than what is currently estimated from ocean models. Recent results obtained at the Indian-Pacific boundary (WOCE line SR3) comfort the idea that a substantial amount of C^{ant} is being stored in the deep Southern Ocean. More studies including models/observations analysis are needed in order to reduce uncertainties attached to global inventories of C^{ant}, especially in the Southern Ocean.

Appendix A

A1. Mixing Model

[39] The multiple end-member mixing model used in this study is based on the optimum multiparametric (OMP) analysis first proposed by *Tomczak* [1981] and further developed in many studies [e.g., *Mackas et al.*, 1987; *Tomczak and Large*, 1989; *Coatanoan et al.*, 1999]. The OMP analysis is an inversion method that uses fields of observed properties in a particular region to determine the relative contribution (mixing ratios) of various source water masses in this region. For every individual sample the model solves a system of linear equations (tracer conservation) by minimizing residuals:

$$A_1 x_1 + A_2 x_2 + A_3 x_3 + \ldots - A_{\text{OBS}} = R_A,$$

$$B_1 x_1 + B_2 x_2 + B_3 x_3 + \ldots - B_{\text{OBS}} = R_B,$$

$$C_1 x_1 + C_2 x_2 + C_3 x_3 + \ldots - C_{\text{OBS}} = R_C.$$

A, B, C… are the ocean tracers used in the model (subscript numbers represent the source waters and OBS stands for tracer measurements). The unknowns (x) are the mixing ratios of source waters 1, 2, 3… determined by minimizing

Table A1. Characteristics of the Six Source Water Types Used in the Mixing Model[a]

End-Members	Salinity	Theta, °C	O$_2$, μmol/kg	PO, μmol/kg
NADW-E	34.86	2.30	235	508
NIDW	34.72	1.70	172	564
Indian Water	34.60	3.50	170	578
WDW/CDW	34.69	0.65	189	597
ISW/WW Weddell	34.60	−2.00	315	638
ISW/WW Prydz	34.60	−2.00	330	670

[a]The eastern North Atlantic Deep Water (NADW-E) and North Indian Deep Water (NIDW) are the deep outflow waters defined by *Broecker et al.* [1985], and Indian Water is the oxygen minimum/nutrients maximum layer described by *Donohue and Toole* [2003]. The southern source waters are Weddell/Circumpolar Deep Water (WDW/CDW), Ice Shelf Water (ISW), and Winter Water (WW) originating from either the Weddell Sea [*Lindegren and Josefson*, 1998; *Hoppema et al.*, 1995, 1999, 2002] or Prydz Bay [*Middleton and Humphries*, 1989; *Wong et al.*, 1998; *Frew et al.*, 1995; *Gibson and Trull*, 1999].

the residuals (*R*) of tracers *A*, *B*, *C*… Two other constraints are added, stating that mixing ratios are positive numbers ($x \geq 0$) and that no other source water contributes to the observed fields of tracers (mass conservation: $\Sigma x = 1$).

[40] In the present study the mixing model was used for two purposes: (1) to determine the mixing ratio of ice-covered surface waters involved in the formation of Antarctic deep and bottom waters (equation (9)) and (2) to localize the cores of North Atlantic Deep Water (NADW) where northern relationships are used to predict preformed DIC and alkalinity (equations (10) and (11)). Six sources were found to be the most appropriate to elucidate those two points (Table A1). These sources are shown on the potential temperature versus salinity and PO plots in Figure A1. The OMP analysis was performed using the CIVA-2 data collected along 30°E in the Southern Ocean and source water masses indicated in Table A1. Results obtained from the OMP analysis are coherent with what is expected from the literature (the two results relevant to our study are shown in Figure A2).

A2. North Atlantic Deep Water

[41] Along 30°E, the North Atlantic component is localized north of 47°S between 2000 and 3500 m (NADW-E > 50%, Figure A2). This result, as well as distributions of the other source water masses defined in Table A1 (results not shown) are coherent with the deep water mass structure described by *Donohue and Toole* [2003] based on a near-synoptic survey of the southwest Indian Ocean. Along WOCE line I5W (32°S in the southwest Indian Ocean), they reported a pronounced salinity maximum lying between 2200 and 3200 m. This salinity maximum layer is identified as NADW flowing from the South Atlantic to the Agulhas-Natal Basin (WOCE line I5W). NADW signal is still well pronounced to the north in the Mozambique Basin (WOCE line I4 along 25°S). *Donohue and Toole* [2003] however noted a slight decrease of dissolved oxygen in NADW flowing to the north which they attribute to the mixing with the overlying oxygen minimum/nutrients maximum layer flowing to the south (Indian Water). In contrast, NADW signature decreases rapidly to the east in the Madagascar Basin (east of 45°E) in the favor of higher oxygen/lower nutrients deep waters flowing from the north Indian Ocean (NIDW) and from the Southern Ocean

(CDW). Below NADW, they also noted the presence of southern waters characterized by high levels of silicate (AABW).

A3. Ice-Covered Surface Waters

[42] The contribution of ice-covered (oxygen depleted) surface waters along 30°E determined from the OMP analysis is about 40–50% in bottom waters south of the ridge and <40% in bottom waters flowing north of the ridge and in Antarctic deep waters (Figure A2). Note that we did not differentiate between the Weddell Sea and Prydz Bay for the mixing ratio of ISW/WW presented in Figure A2 because the mean oxygen depletion under the ice is about the same in the two regions. When differentiating between the two formation regions (results not shown), we found
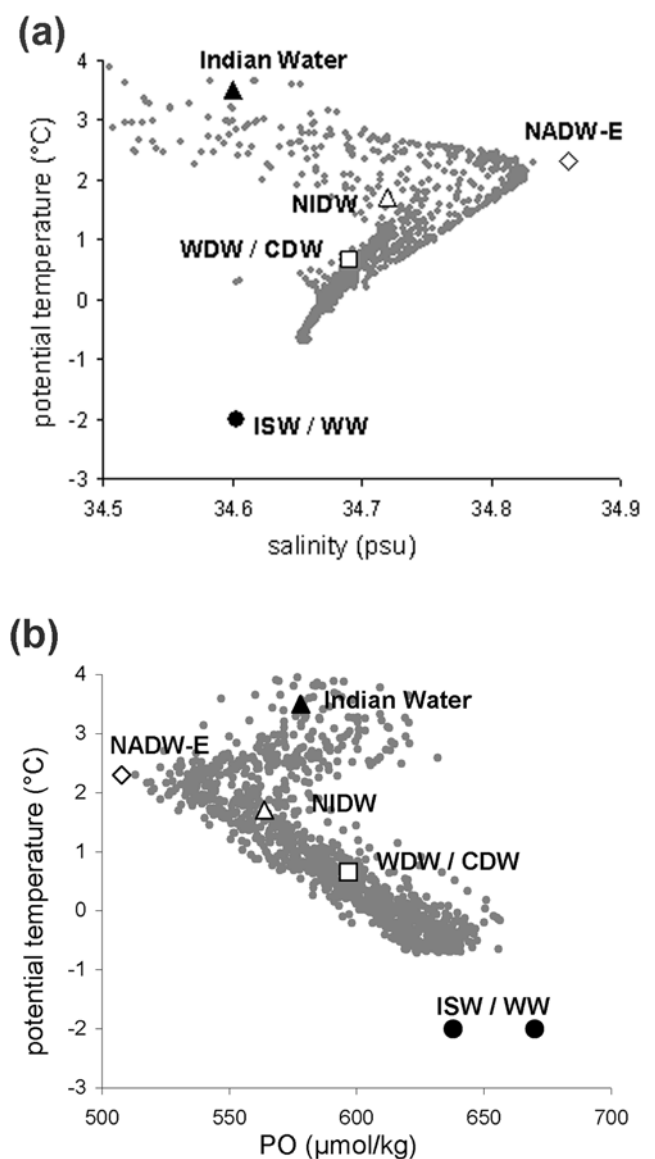

Figure A1. Plots of (a) potential temperature versus salinity and (b) potential temperature versus the conservative tracer PO. Shaded dots are data collected below 500 m during the CIVA-2 cruise (30°E). Characteristics of source waters are from Table A1.
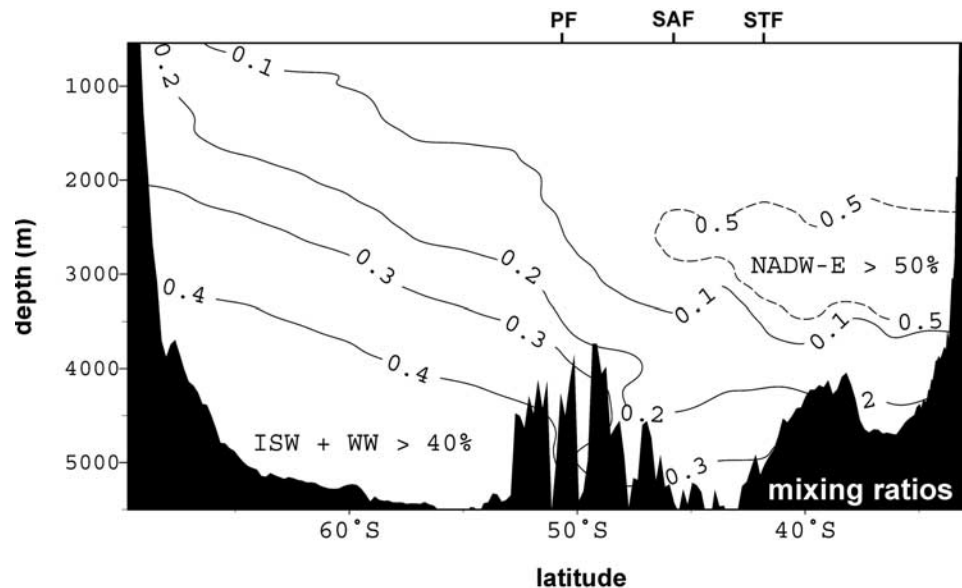
Figure A2. Mixing ratios calculated along 30°E (WOCE line I6). Solid lines show the mixing ratio of ice-covered surface waters involved in the formation of Antarctic Deep and Bottom Waters (ISW and WW from the Weddell Sea and Prydz Bay). The dotted line indicates waters where the northern component dominates (eastern NADW).

that surface waters flowing from the west dominate around 60°S with a mean value of 45% (Weddell ISW/WW in Table A1), whereas the maximum contribution of surface waters flowing from the east (Prydz ISW/WW) was found along the continental slope with a mean value of 35%. These results are in good agreement with hydrological studies conducted in the Weddell Sea and in the vicinity of Prydz Bay based on observations and models [e.g., *Gill*, 1973; *Weiss et al.*, 1979; *Middleton and Humphries*, 1989; *Frew et al.*, 1995; *Wong et al.*, 1998; *Schodlok et al.*, 2001].

[43] Three southern sources are involved in the formation of Antarctic Bottom Water (AABW) and Modified Circumpolar Deep Water (M-CDW): Ice Shelf Water (ISW), Winter Water (WW) and local deep waters (WDW/CDW). Along 30°E, these waters mainly originate from either the Weddell Sea or Prydz Bay. *Weiss et al.* [1979] described the formation of AABW in the Weddell Sea as a two-step process: first, Weddell Sea Bottom Water (WSBW) is formed under the following mixing proportions: 41% ISW, 19% WW and 40% WDW (in agreement with *Gill*, 1973), next WSBW is further diluted by mixing with the local deep water (WDW) to form the classically defined AABW. The final composition of AABW is 26% ISW, 12% WW and 62% WDW (obtained from about 2/3 WSBW and 1/3 WDW). *Middleton and Humphries* [1989] showed that mixing and thermohaline circulation mechanisms operating in Prydz Bay are similar to those in the Weddell Sea. It is therefore not surprising that *Frew et al.* [1995] and *Wong et al.* [1998] calculated about the same composition for Prydz Bay Bottom Water (PPBW) as compared to WSBW (62–64% surface waters and 36–38% deep waters). However, WSBW and PBBW may not mix with the sourrounding deep waters in the same proportion due to the fact that the deep convection appears to be less effective in Prydz Bay than in the Weddell Sea, i.e., the mixing ratio of ice-covered surface waters (ISW and WW) could be lower in Prydz Bay

due to less effective deep convection. Results from the OMP analysis performed along 30°E confirm this idea.

References

Anderson, L. A., and J. L. Sarmiento (1994), Redfield ratios of remineralization determined by nutrient data analysis, *Global Biogeochem. Cycles*, *8*, 65–80.

Anderson, L. G., O. Holby, R. Lindegren, and M. Ohlson (1991), The transport of anthropogenic carbon dioxide into the Weddell Sea, *J. Geophys. Res.*, *96*, 16,679–16,687.

Andreev, A., and S. Watanabe (2002), Temporal changes in dissolved oxygen of the intermediate water in the subarctic North Pacific, *Geophys. Res. Lett.*, *29*(14), 1680, doi:10.1029/2002GL015021.

Archambeau, A.-S., C. Pierre, A. Poisson, and B. Schauer (1998), Distributions of oxygen and carbon stable isotopes and CFC-12 in the water masses of the Southern Ocean at 30°E from South Africa to Antarctica: Results of the Civa1 cruise, *J. Mar. Syst.*, *17*, 25–38.

Benson, B. B., and D. J. Krause (1980), The concentration and isotopic fractionation of gases dissolved in fresh water in equilibrium with the atmosphere: 1, *Oxygen Limnol. Oceanogr.*, *25*, 662–671.

Brewer, P. G. (1978), Direct observation of the oceanic CO$_2$ increase, *Geophys. Res. Lett.*, *5*, 997–1000.

Broecker, W. S. (1974), "NO" a conservative water-mass tracer, *Earth Planet. Sci. Lett.*, *23*, 100–107.

Broecker, W. S. (2001), Carbon futures, in *Geosphere-Biosphere Interactions and Climate*, edited by L. Bengtsson and C. U. Hammer, pp. 66–82, Cambridge Univ. Press, New York.

Broecker, W. S., T. Takahashi, and T. Takahashi (1985), Sources and flow patterns of deep-ocean waters as deduced from potential temperature, salinity, and initial phosphate concentration, *J. Geophys. Res.*, *90*, 6925–6939.

Caldeira, K., and P. B. Duffy (2000), The role of the Southern Ocean in uptake and storage of anthropogenic carbon dioxide, *Science*, *287*, 620–622.

Chen, C.-T. (2001), Comment on "Anthropogenic CO₂ inventory of the Indian Ocean" by C. L. Sabine et al., *Global Biogeochem. Cycles*, *15*, 27–30.

Chen, C. T. A., and F. J. Millero (1979), Gradual increase of oceanic CO₂, *Nature*, *277*, 205–206.

Chen, C. T. A., and R. M. Pytkowicz (1979), On the total CO₂–titration alkalinity–oxygen system in the Pacific Ocean, *Nature*, *281*, 362–365.

Coatanoan, C., N. Metzl, M. Fieux, and B. Coste (1999), Seasonal water mass distribution in the Indian throughflow entering the Indian Ocean, *J. Geophys. Res.*, *104*, 20,801–20,826.

Donohue, K. A., and J. M. Toole (2003), A near-synoptic survey of the southwest Indian Ocean, *Deep Sea Res., Part II*, *50*, 1893–1931.

Frew, R. D., K. J. Heywood, and P. F. Dennis (1995), Oxygen isotope study of water masses in the Princess Elizabeth Trough, Antarctica, *Mar. Chem.*, *49*, 141–153.

Friedlingstein, P., J.-L. Dufresne, P. M. Cox, and P. Rayner (2003), How positive is the feedback between climate change and the carbon cycle?, *Tellus, Ser. B*, *55*, 692–700.

Gibson, J. A. E., and T. W. Trull (1999), Annual cycle of CO₂ under sea-ice and in open water in Prydz Bay, east Antarctica, *Mar. Chem.*, *66*, 187–200.

Gill, A. E. (1973), Circulation and bottom water production in the Weddell Sea, *Deep Sea Res.*, *20*, 111–140.

Gille, S. (2002), Warming of the Southern Ocean since the 1950s, *Science*, *295*, 1275–1277.

Gordon, A. L. (1971), Oceanography of Antarctic waters, *Antarct. Res. Ser.*, *15*, 169–203.

Gordon, A. L. (2003), Oceanography: The brawniest retroflection, *Nature*, *421*, 904–905.

Gruber, N. (1998), Anthropogenic CO₂ in the Atlantic Ocean, *Global Biogeochem. Cycles*, *12*, 165–191.

Gruber, N., J. L. Sarmiento, and T. F. Stocker (1996), An improved method to detect anthropogenic CO₂ in the oceans, *Global Biogeochem. Cycles*, *10*, 809–837.

Holfort, J., K. M. Johnson, B. Schneider, G. Siedler, and D. W. R. Wallace (1998), Meridional transport of dissolved inorganic carbon in the South Atlantic Ocean, *Global Biogeochem. Cycles*, *12*, 479–499.

Hoppema, M., E. Fahrbach, M. Schröder, A. Wisotzki, and H. J. W. De Barr (1995), Winter-summer differences of carbon dioxide and oxygen in the Weddell Sea surface layer, *Mar. Chem.*, *51*, 177–192.

Hoppema, M., E. Fahrbach, M. H. C. Stoll, and H. J. W. De Barr (1999), Annual uptake of atmospheric CO₂ by the Weddell Sea derived from a surface layer balance, including estimations of entrainment and new production, *J. Mar. Syst.*, *19*, 219–233.

Hoppema, M., M. H. C. Stoll, and H. J. W. De Barr (2000), CO₂ in the Weddell Gyre and Antarctic Circumpolar Current: Austral autumn and early winter, *Mar. Chem.*, *72*, 203–220.

Hoppema, M., W. Roether, R. G. J. Bellerby, and H. J. W. De Baar (2001), Direct measurements reveal insignificant storage of anthropogenic CO₂ in the abyssal Weddell Sea, *Geophys. Res. Lett.*, *28*, 1747–1750.

Hoppema, M., H. J. W. De Baar, R. G. J. Bellerby, E. Fahrbach, and K. Bakker (2002), Annual export production in the interior Weddell Gyre estimated from a chemical mass balance of nutrients, *Deep Sea Res., Part II*, *49*, 1675–1689.

Intergovernmental Panel on Climate Change (2001), *Climate Change 2001: The Scientific Basis. Contribution of Working Group I to the Third Assessment Report of the Intergovernmental Panel on Climate Change*, 881 pp., Cambridge Univ. Press, New York.

Ito, T., M. J. Follows, and E. A. Boyle (2004), Is AOU a good measure of respiration in the oceans?, *Geophys. Res. Lett.*, *31*, L17305, doi:10.1029/2004GL020900.

Jabaud-Jan, A., N. Metzl, C. Brunet, A. Poisson, and B. Schauer (2004), Interannual variability of the carbon dioxide system in the southern Indian Ocean (20°S–60°S): The impact of a warm anomaly in austral summer 1998, *Global Biogeochem. Cycles*, *18*, GB1042, doi:10.1029/2002GB002017.

Kara, A. B., P. A. Rochford, and H. E. Hurlburt (2003), Mixed layer depth variability over the global ocean, *J. Geophys. Res.*, *108*(C3), 3079, doi:10.1029/2000JC000736.

Körtzinger, A. (2001), Redfield ratios revisited: Removing the biasing effect of anthropogenic CO₂, *Limnol. Oceanogr.*, *46*, 964–970.

Körtzinger, A., L. Mintrop, and J. C. Duinker (1998), On the penetration of anthropogenic CO₂ into the North Atlantic Ocean, *J. Geophys. Res.*, *103*, 18,681–18,690.

Körtzinger, A., M. Rhein, and L. Mintrop (1999), Anthropogenic CO₂ and CFCs in the North Atlantic Ocean: A comparison of man-made tracers, *Geophys. Res. Lett.*, *26*, 2065–2068.

Lee, K., R. Wanninkhof, R. A. Feely, F. J. Millero, and T.-H. Peng (2000), Global relationships of total inorganic carbon with temperature and nitrate in surface seawater, *Global Biogeochem. Cycles*, *14*, 979–994.

Levitus, S., J. I. Antonov, T. P. Boyer, and C. Stephens (2000), Warming of the world ocean, *Science*, *287*, 2225–2229.

Lindegren, R., and M. Josefson (1998), Bottom water formation in the Weddell Sea resolved by principal component analysis and target estimation, *Chemometrics Intell. Lab. Syst.*, *44*, 403–409.

Mackas, D. L., K. L. Denman, and A. F. Bennett (1987), Least squares multiple tracer analysis of water mass composition, *J. Geophys. Res.*, *92*, 2907–2918.

Mantisi, F., C. Beauverger, A. Poisson, and N. Metzl (1991), Chlorofluoromethanes in the western Indian sector of the Southern Ocean and their relations with geochemical tracers, *Mar. Chem.*, *35*, 151–167.

Matear, R. J., A. C. Hirst, and B. I. McNeil (2000), Changes in dissolved oxygen in the Southern Ocean with climate change, *Geochem. Geophys. Geosyst.*, *1*, doi:10.1029/2000GC000086.

Matear, R. J., C. S. Wong, and L. Xie (2003), Can CFCs be used to determine anthropogenic CO₂?, *Global Biogeochem. Cycles*, *17*(1), 1013, doi:10.1029/2001GB001415.

McCartney, M. S. (1977), Subantarctic Mode Water, *Deep Sea Res.*, *24*, suppl., 103–109.

McNeil, B. I., B. Tilbrook, and R. J. Matear (2001), Accumulation and uptake of anthropogenic CO₂ in the Southern Ocean south of Australia between 1968 and 1996, *J. Geophys. Res.*, *106*, 31,431–31,445.

Meredith, M. P., A. J. Watson, K. A. Van Scoy, and T. W. N. Haine (2001), Chlorofluorocarbon-derived formation rates of the deep and bottom waters of the Weddell Sea, *J. Geophys. Res.*, *106*, 2899–2919.

Metzl, N., B. Moore, and A. Poisson (1990), Resolving the intermediate and deep advective flows in the Indian Ocean by using temperature, salinity, oxygen and phosphates data: The interplay of biogeochemical and geophysical tracers, *Global Planet. Change*, *89*, 81–111.

Metzl, N., B. Tilbrook, and A. Poisson (1999), The annual fCO₂ cycle and the air-sea CO₂ flux in the sub-Antarctic Ocean, *Tellus, Ser. B*, *51*, 849–861.

Middleton, J. H., and S. E. Humphries (1989), Thermohaline structure and mixing in the region of Prydz Bay, Antarctica, *Deep Sea Res., Part A*, *36*, 1255–1266.

Millero, F. J., K. Lee, and M. Roche (1998), Distribution of alkalinity in the surface waters of the major oceans, *Mar. Chem.*, *60*, 111–130.

Orr, J. C., et al. (2001), Estimates of anthropogenic carbon uptake from four three-dimensional global ocean models, *Global Biogeochem. Cycles*, *15*, 43–60.

Orsi, A. H., W. M. Smethie Jr., and J. L. Bullister (2002), On the total input of Antarctic waters to the deep ocean: A preliminary estimate from chlorofluorocarbon measurements, *J. Geophys. Res.*, *107*(C8), 3122, doi:10.1029/2001JC000976.

Pérez, F. F., M. Álvarez, and A. F. Ríos (2002), Improvements on the back-calculation technique for estimating anthropogenic CO₂, *Deep Sea Res., Part I*, *49*, 859–875.

Piola, A. R., and D. T. Georgi (1982), Circumpolar properties of Antarctic Intermediate Water and Subantarctic Mode Water, *Deep Sea Res., Part A*, *29*, 687–771.

Poisson, A., and C. T. A. Chen (1987), Why is there little anthropogenic CO₂ in Antarctic Bottom Water, *Deep Sea Res., Part A*, *34*, 1255–1275.

Rintoul, S. R., and J. L. Bullister (1999), A late winter hydrographic section from Tasmania to Antarctica, *Deep Sea Res., Part I*, *46*, 1417–1454.

Rintoul, S. R., C. W. Hughes, and D. Olbers (2001), The Antarctic Circumpolar Current system, in *Ocean Circulation and Climate*, edited by G. Siedler, J. Church, and J. Gould, pp. 271–300, Elsevier, New York.

Ríos, A. F., X. A. Álvarez-Salgado, F. F. Pérez, L. S. Bingler, J. Arístegui, and L. Mémery (2003), Carbon dioxide along WOCE line A14: Water masses characterization and anthropogenic entry, *J. Geophys. Res.*, *108*(C4), 3123, doi:10.1029/2000JC000366.

Sabine, C. L., and R. A. Feely (2001), Comparison of recent Indian Ocean anthropogenic CO₂ estimates with a historical approach, *Global Biogeochem. Cycles*, *15*, 31–42.

Sabine, C. L., R. M. Key, K. M. Johnson, F. J. Millero, A. Poisson, J. L. Sarmiento, D. W. R. Wallace, and C. D. Winn (1999), Anthropogenic CO₂ inventory of the Indian Ocean, *Global Biogeochem. Cycles*, *13*, 179–198.

Sabine, C. L., R. A. Feely, R. M. Key, J. L. Bullister, F. J. Millero, K. Lee, T.-H. Peng, B. Tilbrook, T. Ono, and C. S. Wong (2002), Distribution of anthropogenic CO₂ in the Pacific Ocean, *Global Biogeochem. Cycles*, *16*(4), 1083, doi:10.1029/2001GB001639.

Schodlok, M. P., C. B. Rodehacke, H. H. Hellmer, and A. Beckmann (2001), On the origin of the deep CFC maximum in the eastern Weddell Sea: Numerical model results, *Geophys. Res. Lett.*, *28*, 2859–2862.

Takahashi, T., W. S. Broecker, and S. Langer (1985), Redfield ratio based on chemical data from isopycnal surfaces, *J. Geophys. Res.*, *90*, 6907–6924.

Takahashi, T., J. Olafsson, J. G. Goddard, D. W. Chipman, and S. C. Sutherland (1993), Seasonal variation of CO$_2$ in the high-latitude surface oceans: A comparative study, *Global Biogeochem. Cycles*, 7, 843–878.

Takahashi, T., et al. (2002), Global sea-air CO$_2$ flux based on climatological surface ocean pCO$_2$, and seasonal biological and temperature effect, *Deep Sea Res., Part II*, 49, 1601–1622.

Thomas, H., and M. H. England (2002), Different oceanic features of anthropogenic CO$_2$ and CFCs, *Naturwissenschaften*, 89, 399–403.

Tomczak, M. (1981), A multi-parameter extension of temperature/salinity diagram techniques for the analysis of non-isopycnal mixing, *Prog. Oceanogr.*, 10, 147–171.

Tomczak, M., and D. G. B. Large (1989), Optimum multiparameter analysis of mixing in the thermocline of the eastern Indian Ocean, *J. Geophys. Res.*, 94, 16,141–16,149.

van Aken, H. M., H. Ridderinkhof, and W. P. M. de Ruijter (2004), North Atlantic deep water in the south-western Indian Ocean, *Deep Sea Res., Part I*, 51, 755–776.

Wallace, D. W. R. (2001a), Introduction to special section: Ocean measurements and models of carbon sources and sinks, *Global Biogeochem. Cycles*, 15, 3–10.

Wallace, D. W. R. (2001b), Storage and transport of excess CO$_2$ in the oceans: The JGOFS/WOCE global CO$_2$ survey, in *Ocean Circulation and Climate*, edited by G. Siedler, J. Church, and J. Gould, pp. 489–520, Elsevier, New York.

Wallace, D. W. R., and K. M. Johnson (1994), Prediction of total dissolved inorganic carbon on basin scales by simple multiple linear regression, *Eos Trans. AGU*, 75, 160.

Wallace, D. W. R., P. Beining, and A. Putzka (1994), Carbon tetrachloride and chlorofluorocarbons in the South Atlantic Ocean, 19°S, *J. Geophys. Res.*, 99, 7803–7819.

Wanninkhof, R., S. C. Doney, T.-H. Peng, J. L. Bullister, K. Lee, and R. A. Feely (1999), Comparison of methods to determine the anthropogenic CO$_2$ invasion into the Atlantic Ocean, *Tellus, Ser. B*, 51, 511–530.

Weiss, R. F., H. G. Östlund, and H. Craig (1979), Geochemical studies of the Weddell Sea, *Deep Sea Res., Part A*, 26, 1093–1120.

WOCE Data Products Committee (2002), WOCE Global Data version 3.0, *WOCE Rep. 180/02*, World Ocean Circ. Exper. Int. Proj. Off., Southampton, U. K.

WOCE Operations Manual (1991), WOCE Hydrographic Programme: Operations and methods, *WHP Off. Rep. WHPPO 91-1, WOCE Rep. 68/91*, WHP Off., Woods Hole, Mass.

Wong, A. P. S., N. L. Bindoff, and A. Forbes (1998), Ocean-ice shelf interaction and possible bottom water formation in Prydz Bay, Antarctica, *Antarct. Res. Ser.*, 75, 173–187.

Wong, A. P. S., N. L. Bindoff, and J. A. Church (1999), Large-scale freshening of intermediate waters in the Pacific and Indian Oceans, *Lett. Nature*, 400, 440–443.

C. Brunet, C. Lo Monaco, N. Metzl, A. Poisson, and B. Schauer, Laboratoire de Biogéochimie et Chimie Marines, Université Pierre et Marie Curie, case 134, 4 place Jussieu, F-75252 Paris Cedex 5, France. (brunet@ccr.jussieu.fr; lomonaco@ccr.jussieu.fr; metzl@ccr.jussieu.fr; apoisson@ccr.jussieu.fr; schauer@ccr.jussieu.fr)